NAVAL POSTGRADUATE SCHOOL
Monterey, California

THESIS

EVALUATION OF IMPROVEMENTS TO AN UNDERWATER ACOUSTIC PROPAGATION MODEL BASED ON THE PARABOLIC EQUATION

by

Kirk A. Weatherly

June 2000

Thesis Advisor: Kevin B. Smith
Second Reader: James V. Sanders

Approved for public release; distribution is unlimited.

REPORT DOCUMENTATION PAGE

Form Approved OMB No. 0704-0188

1. AGENCY USE ONLY *(Leave blank)*	2. REPORT DATE	3. REPORT TYPE AND DATES COVERED
	June 2000	Master's Thesis

4. TITLE AND SUBTITLE
Evaluation of Improvements to an Underwater Acoustic Propagation Model Based on the Parabolic Equation

5. FUNDING NUMBERS

6. AUTHOR(S)
Weatherly, Kirk A.

7. PERFORMING ORGANIZATION NAME(S) AND ADDRESS(ES)
Naval Postgraduate School
Monterey, CA 93943-5000

8. PERFORMING ORGANIZATION REPORT NUMBER

9. SPONSORING / MONITORING AGENCY NAME(S) AND ADDRESS(ES)

10. SPONSORING / MONITORING AGENCY REPORT NUMBER

11. SUPPLEMENTARY NOTES
The views expressed in this thesis are those of the author and do not reflect the official policy or position of the Department of Defense or the U.S. Government.

12a. DISTRIBUTION / AVAILABILITY STATEMENT
Approved for public release; distribution is unlimited.

12b. DISTRIBUTION CODE

13. ABSTRACT *(maximum 200 words)*

This thesis examines two implementations of the parabolic equation approximation to the acoustic wave equation aimed at removing three errors inherent to the wide-angle parabolic equation (WAPE) model. First, the selection of the range-step size used by the split-step Fourier algorithm affects the convergence of the solution. Second, in certain ocean environments WAPE incorrectly computes the down-range transmission loss. Finally, WAPE does not reproduce the standard normal mode basis set as defined by normal mode theory. A double-precision implementation of the WAPE (DP-WAPE) is developed to evaluate the dependence of solution convergence on the numerical precision of the model. Finally, an implementation that is insensitive to the choice of the reference sound speed (COIPE) is evaluated for its ability to reduce or remove the latter two of these three errors. The stability of the WAPE solution was found to be unaffected by the DP-WAPE implementation. The range-step dependence is inherent to the split-step algorithm. The COIPE corrects the transmission loss anomaly and satisfactorily reproduces the standard normal mode basis set.

14. SUBJECT TERMS	15. NUMBER OF PAGES
Underwater Acoustic Propagation, Parabolic Equation Approximation, Modal Decomposition	96
	16. PRICE CODE

17. SECURITY CLASSIFICATION OF REPORT	18. SECURITY CLASSIFICATION OF THIS PAGE	19. SECURITY CLASSIFI- CATION OF ABSTRACT	20. LIMITATION OF ABSTRACT
Unclassified	Unclassified	Unclassified	UL

NSN 7540-01-280-5500

Standard Form 298 (Rev. 2-89)
Prescribed by ANSI Std. 239-18 298-102

Approved for public release; distribution is unlimited

EVALUATION OF IMPROVEMENTS TO AN UNDERWATER ACOUSTIC PROPAGATION MODEL BASED ON THE PARABOLIC EQUATION

Kirk A. Weatherly
Lieutenant, United States Navy
B.S., Old Dominion University, 1992

Submitted in partial fulfillment of the
requirements for the degree of

MASTER OF SCIENCE IN ENGINEERING ACOUSTICS

from the

NAVAL POSTGRADUATE SCHOOL
June 2000

ABSTRACT

This thesis examines two implementations of the parabolic equation approximation to the acoustic wave equation aimed at removing three errors inherent to the wide-angle parabolic equation (WAPE) model. First, the selection of the range-step size used by the split-step Fourier algorithm affects the convergence of the solution. Second, in certain ocean environments WAPE incorrectly computes the down-range transmission loss. Finally, WAPE does not reproduce the standard normal mode basis set as defined by normal mode theory. A double-precision implementation of the WAPE (DP-WAPE) is developed to evaluate the dependence of solution convergence on the numerical precision of the model. Finally, an implementation that is insensitive to the choice of the reference sound speed (COIPE) is evaluated for its ability to reduce or remove the latter two of these three errors. The stability of the WAPE solution was found to be unaffected by the DP-WAPE implementation. The range-step dependence is inherent to the split-step algorithm. The COIPE corrects the transmission loss anomaly and satisfactorily reproduces the standard normal mode basis set.

TABLE OF CONTENTS

I. INTRODUCTION

The fall of the former Soviet Union and the resulting shift in the international political power base has resulted in a dramatic shift in both the content and the application of United States Naval forces during the past decade. The world's largest blue water navy finds itself increasingly involved in green water operations. This shift to littoral waters has brought to the forefront the ever present danger of easily obtainable and extremely capable diesel submarines and shallow water mines. Countries with otherwise limited military resources can acquire the ability to thwart or at the least hinder the application of national objectives. As a result of these changes, numerous efforts toward the development of more accurate acoustic propagation prediction models have arisen. These include areas such as matched-field processing, transient localization, and underwater acoustic communications. Essential to these efforts is the development of acoustic prediction models which can produce both valid and accurate results in highly variable shallow water ocean environments.

A. OCEAN ACOUSTIC MODELING TECHNIQUES

Current acoustic modeling efforts generally fall into one of four broad categories. These are ray models, wavenumber integration techniques, normal mode models, and parabolic equation models. Each of these are based on a variety of approximations to the linear acoustic wave equation. Many of the early models are based on the geometrical limit and define ray trajectories of sound propagation. The resulting ray models can quickly predict pulse propagation travel times and provide rough approximations of the sound field. The limitation of this approach is its reliance on a high-frequency limit which neglects finite-frequency effects such as diffraction. In addition, it has been shown (Smith, et. al., 1992) that the ray equations form a set of coupled, nonlinear equations which suffer from chaotic solutions in the presence of range-dependence. Given the current importance of low-frequency propagation in range-dependent environments, the usefulness of ray models in shallow water media is limited.

Wavenumber integration methods produce highly accurate, full-wave solutions to the wave equation. However, they are

computationaly intensive and are, by design, limited to range-independent environments. They can be quite useful in determining near-field effects but are not of practical utility in predictions of far-field acoustic propagation.

Normal mode models are based on a separation of variables in range and depth of the acoustic wave equation. This approach maintains the full-wave characteristics of the acoustic field, and provides highly accurate results to both simple and complex range dependent ocean environments. The solutions produced are based on the single-frequency Helmholtz wave equation. Due to the computational complexity involved with high frequencies and broadband pulses, as well as range-dependent media, such models are best suited for low-frequency, shallow water environments which support only a small number of propagating modes. The results remain very accurate, but computational time can become counter productive.

The final acoustic modeling technique, and undoubtedly the most popular in range-dependent environments, is based on the parabolic approximation to the Helmholtz wave equation. Numerous marching algorithms have been developed that solve the acoustic field as a boundary value problem. While

it is a one-way wave equation treatment, it is a full-wave model and therefore includes all of the finite-frequency effects of diffraction. Two-way adaptations of parabolic-equation models have been developed, but do not result in significant changes for the majority of shallow water environments of interest. Solutions are, however, still single frequency, requiring multiple solution generation for pulse propagation responses. It is this method that will be the primary focus of this thesis.

B. HISTORY OF THE PARABOLIC EQUATION APPROXIMATION

The parabolic equation (PE) approximation method was first applied to the problem of underwater acoustics by Tappert (1977). Its historical roots are much deeper, however. Breakthroughs in physics and mathematics in the mid-1920's provided the basis for the parabolic wave equation used in acoustics today. The standard parabolic equation (SPE) has the same form as the Schrodinger's equation in quantum mechanics. The earliest documented use of the SPE as an approximation to the theory of wave propagation dates to the mid-1940's and the work of Leontovich and Fock (1946) who originally coined the term "parabolic equation method".

They applied the method to predicting the diffraction on long range tropospheric wave propagation caused by the spherical shape of the earth. Fock (1965) expanded this approach to include high-frequency scattering as well as microwave propagation in waveguides.

With the advent of lasers and their coherent radiation sources in the 1960's, the PE method was further extended to laser beam propagation where it is generally referred to as the "quasi-optical" equation. The quasi-optical equation is most widely used in nonlinear optics where the index of refraction depends on intensity. It is often called the nonlinear Schrodinger's equation. The PE method has also been applied, in more recent years, to the field of fiber optics and plasma physics.

Beam propagation in random media also lends itself well to the PE method. Regardless of the source of the beam -- radio, acoustic, optical -- the problem is analogous to the quantum mechanics problem of motion in a random potential. The radar application of this problem in a randomly fluctuating ionosphere using the split-step Fourier algorithm, discussed later in the next chapter, is covered extensively by Hardin and Tappert (1974).

The most extensive use of the PE approximation to the elliptical wave equation has been in the field of low-frequency underwater acoustic propagation. More than 120 articles and technical reports regarding the PE method and its applications to underwater acoustics were published in the last 15 years. Numerous marching algorithms and computer applications have been constructed with varying degrees of success. The earliest of these were based on the split-step Fourier algorithm (Hardin and Tappert, 1974). In general, these models accept input defining the sound speed, volume loss profiles, and depth contours, and produce output of the acoustic field and associated transmission loss (TL) curves. These results are generally in excellent agreement with experimental measurements for deep ocean environments. The theory behind this method and subsequent attempts to improve it are covered in detail in the next chapter. Since its initial use, the PE method has been extended to include higher acoustic frequencies, random internal-wave fluctuations in the index of refraction, and shallow-water environments with mixed levels of success.

C. ADVANTAGES AND LIMITATIONS OF THE PE METHOD

Long-range, low-frequency sound propagation is generally dominated by rays having small grazing angles since rays propagating at steep angles are greatly attenuated due to penetration and absorption in the seabed. Tappert introduced the PE method, which decomposes an elliptical wave equation into two equations through the separation of outgoing and incoming propagating fields. Tappert's implementation of this method was the first applied to underwater acoustics and is referred to as the standard parabolic equation (SPE). The SPE implementation and many of its more recent incarnations share a number of inherent advantages and limitations.

The advantages of the PE approximation can be divided into three categories (McDaniel, 1975). First, in the long-range, low-frequency environment outlined above, the governing equation can be easily expressed by a parabolic equation, which is easier to solve than either the elliptical or the hyperbolic types. The PE method, therefore, provides a relatively quick solution to long-range, low-frequency, range-dependent problems. Second, in solving the Helmholtz

equation, the problem is posed as a pure boundary value problem. In practice, the determination of the vertical boundary condition is often difficult and imprecise. The PE, however, poses the problem as one of an initial-boundary problem, therefore avoiding the difficulty of the vertical far-end wall boundary condition. Finally, the PE solution is generally cheaper to obtain in both memory and run-time than solving the elliptical equation.

The limitations of the PE method can be placed in one of two broad types. The first of these results from the mathematical formulation of the PE itself which does not allow the inclusion of certain physical phenomenon. The PE is only valid in the far-field and therefore cannot be used for a complete analysis of near-field effects. The index of refraction is assumed to be slowly varying in range. Large and or abrupt changes in the index of refraction can limit the accuracy and validity of results. The PE uses the one-way wave equation and wave propagation from the reverse direction is ignored. Backscattering effects are, therefore, neglected. Treatment of the so-called "square root operator" defines the size of the propagation angle which in turn effects the validity of the PE.

The second type of limitation is defined by the method of solution to the PE. Many of the limitations of this type are specific to the solution algorithm being implemented. The fast Fourier transform works well only for equations with constant coefficients, and therefore must be used with caution. If the boundary is rigid, the algorithm cannot treat it exactly. Finite difference techniques require regular grid partitions. Using the horizontal-interface PE to handle irregular interfaces, unless the sloping angle is small or density change is small, may not produce satisfactory results. In theory, there are no limitations on frequency. In practice, however, using finite difference techniques for high-frequency problems results in intolerable and expensive computational times.

The two types of limitations result in three basic errors. The first error is due to the initial PE approximation. Findings by Smith and Smith (1997) and others show that in the SPE a normal mode will be propagated with the correct amplitude and mode shape but with an error in phase velocity. Some higher order PE approximations improve the accuracy of the phase velocity, but may not properly propagate the mode amplitudes. The error in phase velocity is

addressed in a number of PE approximation methods in the way in which the square root operator is expressed. The second error is introduced by the selection of the range step size. The error is typically found in the second or third order of the range step increment (Jensen, et. al., 1994). If the error is defined as E_n, then for the case of several modes propagating, the error produced in a single range step size would be $E = \sum_n E_n$. The third type of error is due to truncating the field. The initial approximation of the PE poses basic limitations as outlined above. The errors introduced by truncating the field are rooted mainly in computational efficiency in which the numerical results are obtained. A detailed analysis of the effects of range step choice were investigated by Smith (2000).

D. THESIS SUMMARY

The objective of this thesis is to explore the accuracy and validity of various approaches to the PE approximation method as it applies to underwater acoustics, in particular, how each of these methods or implementations affects the

errors outlined above. The resulting accuracy and validity of the model output will be analyzed.

Chapter II, **Theoretical Background**, reviews the theory relevant to the material in the subsequent chapters. Overviews are provided of the parabolic equation approximation used for acoustic propagation modeling, the standard parabolic equation (SPE) method, the wide angle parabolic equation method (WAPE), and the reference sound speed (c_o) insensitive parabolic equation method (COIPE) implementations. Additionally, a brief overview of the method of normal modes is discussed with emphasis on the modal decomposition of acoustic fields generated by PE models.

Chapter III, **Numerical Implementation**, outlines the numerical modeling techniques used in implementing the c_o-insensitive and double-precision WAPE models.

Chapter IV, **Numerical Results**, explores the results obtained from each of the implementations examined. These include SPE, WAPE (single and double precision), and COIPE. Each model is examined for validity and accuracy against a number of standard test cases. The models were also analyzed for their ability to reproduce the standard normal mode basis set.

Chapter V, **Conclusions and Summary**, presents a summation of conclusions and identifies areas of further investigation and research.

II. THEORETICAL BACKGROUND

This chapter outlines the theoretical background supporting the development of the standard, wide-angle, and c_0-insensitive implementations of the parabolic equation (PE) approximation to the acoustic wave equation. The bulk of this theoretical development is directed toward its application in the Monterey-Miami PE (MMPE) implementation of the wide-angle parabolic approximation. The MMPE implementation is emphasized here since it has been subjected to extensive analysis and numerous numerical improvements over its life span. It also serves as the framework of the COIPE model discussed and analyzed later. A summary of the method of normal modes with an emphasis on the modal decomposition of acoustic fields generated by PE models is also included.

The entry point in deriving the PE is the Helmholtz equation, in cylindrical coordinates,

$$\frac{1}{r}\frac{\partial p}{\partial r}\left(r\frac{\partial p}{\partial r}\right) + \frac{1}{r^2}\frac{\partial^2 p}{\partial \varphi^2} + \frac{\partial^2 p}{\partial z^2} + k_0^2 n^2 p = 0 , \qquad (2.1)$$

where $p(r,z)$ is the acoustic pressure, $k_0 = \omega/c_0$ is the reference wavenumber, $n(r, z, \varphi) = c_0/c(r, z, \varphi)$ is the acoustic index of refraction, c_0 is the reference sound speed, and $c(r, z, \varphi)$

is the acoustic sound speed. All of the environmental characteristics are represented in $n(r, z, \varphi)$. The treatment of density contrasts will not be presented here, but is included in the MMPE model by an effective index of refraction term (Smith, 2000). A time-harmonic component of the acoustic field then has the form

$$P(r, z, \varphi, \omega t) = p(r, z, \varphi)e^{-i\omega t}. \tag{2.2}$$

A. OPERATOR NOTATION

In order to develop the various parabolic approximations to the Helmholtz equation, it is useful to introduce an operator notation. Let

$$P_{op} = \frac{\partial}{\partial r} \tag{2.3}$$

and

$$Q_{op} = (\mu + \varepsilon + \upsilon + 1)^{1/2}, \tag{2.4}$$

where $\varepsilon = n^2 - 1$, $\mu = \frac{1}{k_0^2}\frac{\partial^2}{\partial z^2}$, and $\upsilon = \frac{1}{k_0^2 r^2}\frac{\partial^2}{\partial \varphi^2}$. To account for the dominate cylindrical spreading and to simplify the form of the Helmholtz equation, the acoustic pressure may be defined as $p(r, z) = \frac{1}{\sqrt{r}}q(r, z)$, which yields

$$(P_{op}^2 + k_0^2 Q_{op}^2)q = 0 . \tag{2.5}$$

Proper factorization of this equation is accomplished by defining $q = Q_{op}^{-1/2}u$ (Tappert, 1977), such that

$$(P_{op} + ik_0 Q_{op})(P_{op} - ik_0 Q_{op})u + ik_0[P_{op}, Q_{op}]u = 0 . \tag{2.6}$$

The commutator $[P_{op}, Q_{op}]$ is exactly zero for layered media, and is assumed negligible. The remaining factors of Eq. (2.6) define the wave equations for the incoming and outgoing fields, the latter of which then satisfies

$$P_{op}u = ik_0 Q_{op}u \tag{2.7}$$

or

$$-ik_0^{-1}\frac{\partial u}{\partial r} = Q_{op}u . \tag{2.8}$$

In cases where backscattered energy may be neglected, Eq. (2.8) provides the full description of the forward propagating acoustic energy.

B. THE SPLIT-STEP FOURIER ALGORITHM

The most common methods of computing PE solutions are (1) the finite element method (Collins, 1994), (2) the implicit finite difference method (Lee, et. al., 1981), and (3) the split-step Fourier (PE/SSF) method (Hardin and Tap-

pert, 1973). Of these three methods, the PE/SSF method has the distinct advantage of speed. This is accomplished by decomposing the acoustic field into a slowly modulating envelope function and a phase term which oscillates with the acoustic frequency. Defining $u = \Psi e^{ik_0 r}$ and substituting into Eq. (2.8) yields

$$\frac{\partial \Psi}{\partial r} = -ik_0 \Psi + ik_0 Q_{op} \Psi = -ik_0 H_{op} \Psi , \tag{2.9}$$

where $H_{op} = 1 - Q_{op}$ is a Hamiltonian-like operator which defines the evolution of the PE field function in range.

In order to compute the solution to the acoustic field, a marching algorithm must be developed of the form

$$\Psi(r + \Delta r) = \Phi(r)\Psi(r) . \tag{2.10}$$

The propagator, $\Phi(r)$, is designed to propagate the solution out in range. The PE/SSF method accomplishes this via

$$\Phi(r) \approx e^{-ik_0 \bar{H}_{op}(r)\Delta r} \tag{2.11}$$

where

$$\bar{H}_{op}(r) = \frac{1}{\Delta r} \int_{r}^{(r+\Delta r)} H_{op}(r')dr' . \tag{2.12}$$

In practice, the Hamiltonian is usually considered constant over a small range-step such that $H_{op}(r) \approx H_{op}(r)$.

The operator H_{op} (and Q_{op}) is not a scalar operator but a combination of scalar and differential operators. Each individual operator within H_{op} can, however, be applied by a simple scalar multiplication in the proper domain. Therefore, each of the terms of H_{op} must be separated in order to comply with the PE/SSF algorithm. This necessitates the approximation of the square-root operator, specifically

$$H_{op}\left(\frac{\partial^2}{\partial z^2}, \frac{1}{r^2}\frac{\partial^2}{\partial \phi^2}, n(r,z)\right) \approx T_{op}\left(\frac{\partial^2}{\partial z^2}\right) + U_{op}(n(r,z)) + V_{op}\left(\frac{1}{r^2}\frac{\partial^2}{\partial \phi^2}\right). \qquad (2.13)$$

It is this approximation that forms the basis of numerous higher-order PE model implementations.

If the uncoupled azimuth approximation is employed then $V_{op} = 0$ identically. The U_{op} is a multiplication operator in z-space and is therefore a diagonal matrix. The operator T_{op} is not diagonal in z-space, resulting in different eigenfunctions being coupled. The T_{op} is, however, diagonal in vertical wavenumber space. It is advantageous then to treat each operator separately, one in k_z-space, and the other in z-space. Employing the Baker-Campbell-Hausdorff expansion (Bellman, 1964),

$$e^{A+B} = e^A e^B e^{[A,B]+[A,[A,B]]+[B,[B,A]]+\cdots}, \qquad (2.14)$$

where $A = -ik_0\Delta r T_{op}$ and $B = -ik_0\Delta r U_{op}$. T_{op} and U_{op} are both small, therefore it is assumed their products of second order are negligible. Using Eq. (2.14), $\Phi(r)$ becomes

$$\Phi(r) = e^{-ik_0\frac{\Delta r}{2}U_{op}(r+\Delta r)} e^{-ik_0\Delta r T_{op}} e^{-ik_0\frac{\Delta r}{2}U_{op}(r)}. \qquad (2.15)$$

Third order accuracy results from this centered step scheme (Jensen, et. al., 1994). Due to the formulation of the propagator there are no intrinsic losses due to the numerical scheme and energy conservation is retained (Tappert, 1995).

In summary, the PE/SSF algorithm accepts the PE field function Ψ specified at some range r in the z-domain. This is followed by a multiplication of $e^{-ik_0\frac{\Delta r}{2}U_{op}(r)}$, the z-space operator defined at the beginning of the range-step. This product is then transformed to the k_z-domain and multiplied by $e^{-ik_0\Delta r\hat{T}_{op}(k_z)}$, the k_z-space operator. Another transformation to the z-domain and multiplication by the z-space operator $e^{-ik_0\frac{\Delta r}{2}U_{op}(r+\Delta r)}$, defined at the end of the range-step, produces the final resultant field function at $r+\Delta r$ in the z-domain. Note that the FFT convention used here and in the numerical implementations is

$$\hat{\Psi}(z) = \mathrm{FFT}(\Psi(k_z)) \quad , \tag{2.16}$$
$$\Psi(k_z) = \mathrm{IFFT}(\hat{\Psi}(z)) \quad .$$

Wrapping these steps into a single equation results in

$$\Psi(r+\Delta r, z) = \tag{2.17}$$
$$e^{-ik_0\frac{\Delta r}{2}U_{op}(r+\Delta r, z)} \times \mathrm{FFT}\left\{ e^{-ik_0\Delta r\hat{T}_{op}(k_z)} \times \mathrm{IFFT}\left[e^{-ik_0\frac{\Delta r}{2}U_{op}(r, z)} \times \Psi(r, z) \right] \right\} \quad .$$

C. STANDARD PE DEVELOPMENT

The lowest order approximation to the Hamiltonian operator is commonly referred to as the standard parabolic equation (SPE). This approximation is obtained by assuming the operators are small,

$$\varepsilon \ll 1 \text{ and } \mu \ll 1 \quad . \tag{2.18}$$

The first of these is merely a recognition that sound speeds vary by less than 2% in most ocean environments, so $n(r, z) \approx 1$ everywhere. The second assumption can be seen to imply that vertical angles $\left(\frac{k_z^2}{k_0^2} \approx \sin^2\theta\right)$ are small. This limits the SPE accuracy to small angles.

With these approximations, the SPE is obtained by a binomial expansion of the square root operator,

$$H_{spe} = 1 - \left(1 - \frac{1}{2}\mu - \frac{1}{2}\varepsilon\right) = -\frac{1}{2}\mu - \frac{1}{2}\varepsilon \,. \tag{2.19}$$

The separated operators then have the form

$$T_{spe}\left(\frac{\partial^2}{\partial z^2}\right) = -\frac{1}{2k_0^2}\frac{\partial^2}{\partial z^2} \tag{2.20}$$

and

$$U_{spe}(r, z) = -\frac{1}{2}(n^2(r, z) - 1) \,. \tag{2.21}$$

Note that in the context of H_{spe} acting as a Hamiltonian operator, the operators T_{spe} and U_{spe} correspond to kinetic and potential energy operators, respectively. In the vertical wavenumber domain,

$$\hat{T}_{spe}(k_z) = \frac{1}{2}\frac{k_z^2}{k_0^2} \,. \tag{2.22}$$

D. WIDE-ANGLE PE DEVELOPMENT

A higher order approximation to the operators was introduced by Thompson and Chapman (1983) and is often referred to as the wide-angle PE (WAPE) approximation. The operators of the WAPE are defined by

$$T_{wape}\left(\frac{\partial^2}{\partial z^2}\right) = 1 - \left[1 + \frac{1}{k_0^2}\frac{\partial^2}{\partial z^2}\right]^{1/2} \tag{2.23}$$

and

$$U_{wape}(r, z) = -(n(r, z) - 1) . \tag{2.24}$$

In wavenumber space, the WAPE kinetic energy operator takes the form of

$$\hat{T}_{wape}(k_z) = 1 - \left[1 - \left(\frac{k_z}{k_0}\right)^2\right]^{1/2} . \tag{2.25}$$

Note that energy propagating at angles beyond vertical, $k_z > k_0$, is evanescent since

$$\hat{T}_{wape}(k_z > k_0) = 1 - i\left[\left(\frac{k_z}{k_0}\right)^2 - 1\right]^{1/2} . \tag{2.26}$$

The wide-angle PE, and other higher-order approximations to the SPE, was originally developed in an effort to extend the region of validity of the SPE. While the wide-angle PE succeeded in this goal, it introduced a number of other issues. These include a sensitivity to the selection of the reference sound speed and an inability to reproduce the standard normal mode basis set. This said, however, the wide-angle approximation has been very successful in producing useful and valid results in many situations. The following section addresses an attempt to mitigate the reference sound speed sensitivity experienced by the WAPE approximation.

E. COIPE DEVELOPMENT

WAPE and other higher-order models are not exact representations and may under certain circumstances produce results worse than the SPE which they are meant to improve upon (Porter and Jensen, 1993). In these cases, it is often found that the error results from errors in the underlying normal mode basis set, their associated phase speeds, and a sensitivity to the choice of reference sound speed, c_0. The choice of c_0 is the one ambiguous feature of all PE models. Due to this ambiguity, it is desirable to develop a model that is insensitive to the input reference sound speed. Then, any significant deviations in the choice of c_0 would not adversely affect the computed results. In an attempt to develop a wide angle implementation that is insensitive to c_0, Tappert (1991) developed the c_0-insensitive PE (COIPE) approximation.

The COIPE approximation based on the WAPE approximation with the operator replacement

$$\frac{1}{k_0^2}\frac{\partial^2}{\partial z^2} \rightarrow \frac{1}{k_0(r)}\frac{\partial}{\partial z} n^{-1}(r, z) \frac{1}{k_0(r)}\frac{\partial}{\partial z}, \tag{2.27}$$

where $k_0(r)$ is now range-dependent due to the range-dependent nature of the reference sound speed, $c_0(r)$. Introducing the operator

$$\hat{p}(r) = -\frac{i}{k_0(r)}\frac{\partial}{\partial z}, \tag{2.28}$$

the c_0-insensitive approximation to the Hamiltonian operator becomes

$$H_{Ins}(r, z) = (1 - n(r, z)) + (1 - \sqrt{1 - \hat{p}(r)n^{-1}(r, z)\hat{p}(r)}) . \tag{2.29}$$

In this form the spherical wavefront property of the TC approximation is maintained for steep angles. Furthermore, this approximation is not sensitive to the choice of c_0, and reduces to a c_0-independent approximation for small angles (Tappert, 1977). The resulting wave equation approximation is

$$\frac{\partial \Psi}{\partial r} = -ik_0 H_{Ins}(r)\Psi . \tag{2.30}$$

To implement this approach, a transform to a new depth coordinate is necessary. The transformation relationships are

$$\tilde{z} = \int_0^z \sqrt{n(z, r')}dr' , \tag{2.31}$$

$$n(z, r) = n(z, r) , \tag{2.32}$$

and

$$\tilde{\Psi}(\tilde{z}, r) = n^{-1/4}(z, r)\Psi(z, r) . \tag{2.33}$$

The corresponding Hamiltonian operator then becomes

$$\tilde{H}(r) = (1 - \tilde{n}(\tilde{z}, r)) + (1 - \sqrt{1 - \tilde{p}^2(r)}) . \tag{2.34}$$

Note that in the tilde-domain this has the same form as the TC operator. The resulting form of the parabolic wave equation in the tilde domain is

$$\frac{\partial}{\partial r}\tilde{\Psi} = ik_o\tilde{H}_{Ins}(r)\tilde{\Psi} . \tag{2.35}$$

The corresponding kinetic and potential energy operators of the COIPE in the tilde-domain may then be represented by

$$\tilde{T}_{Ins}(r, k_{\tilde{z}}) = 1 - \sqrt{1 - \frac{1}{k_o^2(r)}\frac{\partial^2}{\partial\tilde{z}^2}} \tag{2.36}$$

and

$$\tilde{U}_{Ins}(r, \tilde{z}) = 1 - \tilde{n}(r, \tilde{z}) . \tag{2.37}$$

The COIPE requires, in general, the computation of c_0 for each range step. To compute c_0, the condition that the water depth be unchanged in the z coordinate must be satisfied. This is accomplished via

$$h(r) = \int_0^{h(r)} \sqrt{n(z,r)}\,dz\,, \tag{2.38}$$

where h(r) is the water depth at range r. Under this condition, the reference sound speed is

$$c_0(r) = \left(\frac{1}{h(r)} \int_0^{h(r)} \frac{1}{\sqrt{c(z,r)}}\,dz \right)^{-2}\,. \tag{2.39}$$

The University of Miami PE/SSF acoustic model (UMPE) has been tested using the technique outlined above with excellent results (Tappert, 1995). A numerical implementation of the COIPE within the existing framework of the MMPE model is covered in the following chapter. Comparative analysis of this approach with the SPE, MMPE, and selected normal mode test cases is covered in Chapter IV.

F. NORMAL MODE FUNCTIONS AND THEIR DECOMPOSITION FOR THE PE APPROXIMATION

One of the difficulties encountered with the WAPE approximation is that it does not decompose into the standard normal mode basis set as defined by normal mode theory and the SPE. Thomson (1993) looked at this problem for the SPE approximation. He showed that the field p that satisfies

the acoustic wave equation exactly relates to the field Ψ satisfying the SPE approximation. The wavenumber of Ψ and the modal amplitudes may be determined exactly. The corresponding normal mode amplitudes and wavenumbers are then obtained. The WAPE, however, has modal eigenfunctions and eigenvalues of Ψ distinct from the acoustic wave equation.

Smith and Smith (1997) showed that the modal decomposition of solutions based on the WAPE generated erroneously range-dependent mode amplitudes in a range-independent environment. This was due to the mismatch between the standard normal mode basis set (based on the Helmholtz equation) and the proper basis set of the WAPE. Furthermore, they were able to develop an approximate numerical scheme for computing the proper WAPE basis set. This resulted in the proper range-independent character of the mode amplitudes. Additionally, they suggested that the higher-order COIPE version of the WAPE might overcome such issues and decompose properly into the standard normal mode basis set. This will be one of the primary tests of the improved accuracy of the COIPE over the WAPE.

Normal modes are obtained by using the method of separation of variables. As presented here, it assumes the ocean

is horizontally stratified, is of constant water density, is azimuthally symmetric, and is range-independent. As was presented for the PE, the time harmonic acoustic field $p(r,z)e^{-i\omega t}$ at $r>0$ due to a point source at $z = z_s$ and $r = 0$ satisfies the 2D Helmholtz equation (no azimuthal variations possible)

$$\frac{1}{r}\frac{\partial}{\partial r}\left(r\frac{\partial p}{\partial r}\right) + \frac{\partial^2 p}{\partial z^2} + k_0^2 n^2(z) p = 0 . \tag{2.40}$$

For solutions of the form $p(r,z) = \frac{1}{\sqrt{r}}\phi(r)v(z)$, the depth-dependent modal equation

$$\frac{d^2}{dz^2}v_m(z) + (k_0^2 n^2(z) - K_m^2)v_m(z) = 0 \tag{2.41}$$

is obtained. Here, K_m^2, the square of the horizontal wavenumber for mode m, is the separation constant (eigenvalue) and $v_m(z)$ is the specific mode function (eigenfunction) associated with the separation constant. Given an arbitrary pressure field, the sum of the normal modes is required and is expressed as

$$p(r,z) = \frac{1}{\sqrt{r}}\sum_{m=1}^{\infty}\phi_m(r)v_m(z) , \tag{2.42}$$

where the cylindrical spreading factor has been explicitly included. The factor $\phi_m(r)$ can easily be shown to have the form of a Hankel function scaled by mode excitation values depending on the source strength and depth in the waveguide. In the far-field, the only range-dependence of this function is in the phase (having already accounted for cylindrical spreading). Thus, a generalized mode amplitude, $A_m(r)$, may be defined according to

$$p(r,z) = \frac{1}{\sqrt{r}}\sum_m A_m(r)\nu_m(z)\,. \tag{2.43}$$

The normalized eigenfunctions form a complete, orthogonal basis set, defined by

$$\frac{1}{\rho(z)}\int_0^D \nu_n(z)\nu_m(z)dz = \delta_{mn}\,. \tag{2.44}$$

Thus, by using the orthogonality relation and assuming normalized modes, the generalized modal amplitudes can be extracted from the computed pressure field by forming an inner-product

$$A_m(r) = \sqrt{r}\int_0^D \frac{p(r,z)\nu_m(z)}{\rho(z)}dz\,. \tag{2.45}$$

This technique is used in the analysis and comparisons of the normal mode amplitudes of the SPE, WAPE, and COIPE models in Chapter IV.

Finally, the corresponding depth separated equations of the various parabolic approximations introduced should be examined. First, note that the normal mode equation, Eq. (2.41), may be written in terms of the operators μ and ε (defined in Eq. (2.4)) as

$$(\mu+\varepsilon)v_m = \left(\frac{K^2_m}{k^2_0} - 1\right)v_m . \tag{2.46}$$

This indicates that the basis set, v_m, are eigenfunctions of the combined operator $(\mu+\varepsilon)$ with eigenfunctions $(K^2_m/k^2_0 - 1)$.

The PE approximation has a depth separated equation of the form

$$H_{op}\chi_m = i\frac{K_m}{k_0}\chi_m , \tag{2.47}$$

where the functions χ_m are the eigenfunctions of the corresponding PE approximation. In order for the eigenfunctions χ_m and v_m to be the same (up to some normalization factors), the operator H_{op} must be some rational function of the operator $(\mu+\varepsilon)$. For example, a simple polynomial series with

terms $(\mu+\varepsilon)^n$, where n is some integer, will have the same basis set v_m.

The standard parabolic equation is a simple first order binomial expansion of the Hamiltonian operator, i.e.

$$H_{spe} = -\frac{1}{2}(\mu+\varepsilon). \tag{2.48}$$

This obviously satisfies the above criterion, therefore the SPE approximation has the same normal mode basis set as the fundamental Helmholtz equation.

The wide-angle PE, on the other hand, may be written in the form

$$H_{wape} = 2-\sqrt{1+\mu}-\sqrt{1+\varepsilon}. \tag{2.49}$$

Performing a power series expansion on this operator to second order yields

$$H_{wape} \approx -\frac{1}{2}(\mu+\varepsilon)+\frac{1}{8}(\mu^2+\varepsilon^2). \tag{2.50}$$

This shows that the WAPE approximation is only first order accurate in the operator $(\mu+\varepsilon)$ but has errors in the second order terms. It is this weakness of the WAPE which generates some of the associated problems with this approximation.

The c_0-insensitive PE approximation, however, may be written as

$$H_{Ins} = 2 - \sqrt{1 + \frac{\mu}{\sqrt{1+\varepsilon}}} - \sqrt{1+\varepsilon}\,. \tag{2.51}$$

A power series expansion of this operator to third order yields

$$H_{Ins} \approx -\frac{1}{2}(\mu+\varepsilon) + \frac{1}{8}(\mu+\varepsilon)^2 - \frac{1}{16}(\mu+\varepsilon)^3 + \frac{\mu^2\varepsilon}{16}\,. \tag{2.52}$$

Thus, the COIPE is accurate to second order in $(\mu+\varepsilon)$ with leading error in the third order terms. This was first shown by Tappert and Brown (1996). It is this feature of the COIPE which makes it an attractive alternative to the WAPE approximation. As will be shown, this also generates solutions which may be decomposed into the standard normal mode basis set without significant error.

THIS PAGE INTENTIONALLY LEFT BLANK

III. NUMERICAL IMPLEMENTATION

This chapter outlines the numerical implementation of the PE models used in the analysis of the c_0-insensitive PE approximation (COIPE) as well as a double-precision version of the MMPE. The MMPE (Smith, 2000) is an existing well-documented version of the WAPE approximation. In the cases where a SPE solution was required for comparison purposes, the operators U_{wape} and $\hat{T}_{wape}$ were replaced with U_{spe} and $\hat{T}_{spe}$ within the framework of the MMPE model. As was discussed in the previous chapter, the COIPE implementation strives to eliminate the sensitivity to the chosen reference sound speed suffered by the WAPE approximation. As will be shown in the next chapter, a small change in the specified reference sound speed can result in a dramatic change in the predicted acoustic field. This error often increases with range and for complex, highly range-dependent environments can quickly result in the produced data being unusable. The numerical implementation described here was chosen such that it could be easily integrated into the existing MMPE model to provide the most reliable comparison of results. The

results of these comparisons are discussed in the following chapter.

A. ENVIRONMENTAL GRID SIZES

The MMPE, as well as the COIPE, implementation discussed here uses a discretized grid to describe the environment. The grid step-sizes are user definable and can dramatically affect the solution obtained by the model. The grid sizing method described here is that used by the MMPE model as well as the COIPE implementation of the MMPE. The environment is discretized by a mesh of size $(\Delta r, \Delta z)$. This results in the field and propagator functions being discretized in depth with array length N, where N is the corresponding length of the FFT used in the PE/SSF algorithm. In other words,

$$\Psi(r, z) \Rightarrow \Psi(r_i, z_n), \tag{3.1}$$

where

$$r_i = (i-1)\Delta, \quad i = 1 \ldots i_{max}, \tag{3.2}$$

and

$$z_n = \begin{cases} \left(n - \frac{1}{2}\right)\Delta z, & n = 1, \frac{N}{2} \\ -\left(N - n + \frac{1}{2}\right)\Delta z, & n = \frac{N}{2} + 1, N \end{cases} . \tag{3.3}$$

The depth mesh is defined such that grid points lie on fractional values of Δz. This convention results in the avoidance of carrying the zero-pressure value at $z = 0$ throughout the calculations. It should be noted that because of using the full Fourier transform, half of the depth mesh values define an image ocean for negative depths. This has the added benefit of enforcing the surface boundary condition, defined in the next section, via FFT symmetry. Analysis by Tappert (1977) and Smith (2000) showed that by considering a lower limit on the allowable angles of propagation, a default value of Δz may be defined and therefore a default transform size N. This is possible since the depth mesh influences the wavenumber increments Δk_z via the FFT. For a given environment with a relatively small angle of propagation, the mesh size may be increased. An increase in the mesh size results in a corresponding decrease in the computational time. As propagation angles increase, the mesh size is reduced. The most accurate solution, therefore,

should be obtained when both Δz and Δr are on the order of a wavelength.

B. TILDE TRANSFORMATION AND C_0 GENERATION

The tilde transformation begins by defining a rescaled depth variable z in terms of the true depth z

$$\tilde{z} = \int_0^z \sqrt{n(z', r)}\, dz' . \tag{3.4}$$

If it is required that the bottom depth remains fixed, in other words that $z_b = z_b = h$, then the range-dependent bottom depth is

$$h(r) = \int_0^{h(r)} \sqrt{n(z', r)}\, dz' = \int_0^{h(r)} \sqrt{\frac{c_0(r)}{c(z', r)}}\, dz' = \sqrt{c_0(r)} \int_0^{h(r)} \frac{1}{\sqrt{c(z', r)}}\, dz' , \tag{3.5}$$

where c_0 has been specifically declared as range-dependent, due either to h(r) or c(z,r). Solving for $c_0(r)$,

$$c_0(r) = \left[\frac{1}{h(r)} \int_0^{h(r)} \frac{1}{\sqrt{c(z', r)}}\, dz' \right]^{-2} . \tag{3.6}$$

This expression defines the rang-dependent reference sound speed to be used in the parabolic approximation. Its decla-

ration then eliminates the need for a user-defined value. Furthermore, since the definition is based on an evaluation of the local environment at each range, it will preserve reciprocity.

If c(z) varies linearly with depth,

$$c(z) = c(z_{i-1}) + b(z - z_{i-1}) = a + bz\,, \tag{3.7}$$

where b is the sound speed gradient,

$$b = \frac{c(z) - c(z_{i-1})}{z - z_{i-1}}\,, \tag{3.8}$$

and

$$a = c(z_{i-1}) - bz_{i-1}\,, \tag{3.9}$$

then the integral may be written

$$\int_{z_{i-1}}^{z_i} \frac{1}{\sqrt{c(z')}}dz' = \int_{z_{i-1}}^{z_i} \frac{1}{\sqrt{a + bz'}}dz'\,. \tag{3.10}$$

Using a table of integrals, this becomes

$$2\frac{\sqrt{a + bz'}}{b}\Bigg|_{z_{i-1}}^{z_i} = \frac{2}{b}[\sqrt{a + bz_i} - \sqrt{a + bz_{i-1}}]\,. \tag{3.11}$$

Substituting into Eq. (3.11) for a and b,

$$\int_{z_{i-1}}^{z_i} \frac{1}{\sqrt{c(z')}}dz' = \frac{2(z_i - z_{i-1})}{(c_i - c_{i-1})}(\sqrt{c_i} - \sqrt{c_{i-1}}) = \frac{2(z_i - z_{i-1})}{\sqrt{c_i} + \sqrt{c_{i-1}}}\,. \tag{3.12}$$

Now consider the sampling of the environment within the model. The typical definitions are

$$z_k = \left(k - \frac{1}{2}\right)\Delta z \ , \qquad (3.13)$$
$$k = 1, 2, 3 \ldots \frac{N}{2} \ ,$$

where N is the FFT size. Based on this grid sampling of the environment, it would then be unusual if $z_{nbi} = h(r)$. Rather, the bottom lies just below the index

$$nbi = int\left(\frac{h(r)}{\Delta z}\right), \qquad (3.14)$$

such that $z_{nbi} \leq h(r)$. To perform the integrals needed, however, the conditions

$$z_1 = 0 \ , \qquad (3.15)$$
$$z_{Ns} = h(r) \ ,$$

must be satisfied. This may be accomplished by first transforming to a z_j space (which is not equally spaced), which satisfies Eq. (3.15), and then interpolating z_j to z_k where

$$\tilde{z}_k = \left(k - \frac{1}{2}\right)\Delta z \ . \qquad (3.16)$$

Part of the difficulty is to define the sound speed on the non-grid points z = 0 and z = h(r). Fortunately, this is essentially already accomplished in the MMPE model. The

surface sound speed is required as an input to the MMPE, and is stored in the sound speed array by the environmental propagator subroutine. The sound speed at the bottom depth, h(r), is also already estimated at the grid point nbi. While this is an estimate, it provides a good approximation for cases where energy doesn't significantly interact with the bottom. This results in

$$\begin{aligned} \tilde{z}_1 &= 0 \Rightarrow z = 0 \Rightarrow c(0) = SS \ , \\ \tilde{z}_{Ns} &= h(r) \Rightarrow z = h(r) \Rightarrow c(h(r)) = SSBW \ , \end{aligned} \tag{3.17}$$

where SS0 is the surface sound speed input into MMPE and SSBW is the estimated water sound speed at the water/bottom interface.

The numerical scheme for computing c_0 and the tilde transformation can now be defined. Using Eqs. (3.6) and (3.12),

$$c_0(r) = \tag{3.18}$$

$$\frac{h^2(r)}{4}\left\{\left[\frac{z_1}{\sqrt{c_1}+\sqrt{SS0}}\right]+\left[\sum_{k=2}^{nbi}\frac{z_k - z_{k-1}}{\sqrt{c_k}+\sqrt{c_{k-1}}}\right]+\left[\frac{h(r)-z_{nbi}}{\sqrt{SSBW}+\sqrt{c_{nbi}}}\right]\right\}^{-2} ,$$

where it is assumed that the sound speed has already been interpolated onto the gridded mesh z_k at values c_k. Similarly, Eq. (3.4) with $z_1 = 0$ becomes

$$\tilde{z}_2 = 2\sqrt{c_0}, \tag{3.19}$$

$$\tilde{z}_j = \tilde{z}_{j-1} + 2\sqrt{c_0}\frac{z_k - z_{k-1}}{\sqrt{c_k} + \sqrt{c_{k-1}}},\ j = 3 \ldots nbi + 1,$$

$$\tilde{z}_{Ns} = \tilde{z}_{Ns-1} + 2\sqrt{c_0}\frac{h - z_{nbi}}{\sqrt{SSBW} + \sqrt{c_{nbi}}} .$$

Note that $Ns = nbi + 2$ since the points $z = 0$ and $z = h$ have been added. As a result of this transformation and the above definitions,

$$\begin{aligned} \tilde{c}_1 &= SS, \\ \tilde{c}_{Ns} &= SSBW, \\ \tilde{c}_{j \neq 1, Ns} &= c_{j-1} . \end{aligned} \tag{3.20}$$

Given these relationships, it is now necessary to interpolate in depth the tilde domain sound speed onto the standard grid. Defining

$$\begin{aligned} \tilde{z}_k &= \left(k - \frac{1}{2}\right)\Delta z , \\ k &= 1, 2, \ldots, \frac{N}{2} , \end{aligned} \tag{3.21}$$

it is desired that

$$c(z_k) = c(\tilde{z}_k) . \tag{3.22}$$

A simple linear interpolation from $c(z_j)$ to $c(z_k)$ could be performed. This, however, would not preserve the linear gradient nature of $c(z_k)$, and the relation defined by Eq. (3.22) would not be satisfied. Instead, assume

$$z_{j-1} \le z_k < z_j , \tag{3.23}$$

and then define the fractional depth as

$$f_k = \frac{z_k - z_{j-1}}{z_j - z_{j-1}} . \tag{3.24}$$

Tappert (1995) shows that the inversion of the mapping needed produces

$$c_k = c_{j-1} + g_k(c_j - c_{j-1}) , \tag{3.25}$$

where

$$g_k = \frac{f_k}{\sqrt{c_j} + \sqrt{c_{j-1}}}[2\sqrt{c_{j-1}} + (\sqrt{c_j} - \sqrt{c_{j-1}})f_k] . \tag{3.26}$$

C. ACOUSTIC FIELD GENERATION

In the MMPE model the source amplitude is defined relative to a small finite distance from the source. This is done to avoid the singularity at range $r = 0$ in

$$p = P_0\sqrt{\frac{R_0}{r}}\Psi e^{ik_0 r} . \tag{3.27}$$

Therefore, the source is defined such that $p(r = R_0) = P_0$. The reference range is defined to be one meter to remain consistent with most sonar equations. Using this convention, the source level is related to P_0 by

$$SL = 20\log\left(\frac{P_0}{P_r}\right) \text{ dB re } P_r\ R_0 \tag{3.28}$$

where $P_r = 1\ \mu Pa$ at the reference range of R_0.

The form of the source field $\Psi(r = 0, z)$ must now be determined. Rewriting Eq. (3.27) as

$$\Psi(r, z)e^{ik_0 r} = \frac{1}{P_0}\sqrt{\frac{r}{R_0}}p(r, z), \tag{3.29}$$

then

$$\Psi(r = 0, z) = \lim_{r \to 0} \frac{1}{P_0}\sqrt{\frac{r}{R_0}}p(r, z), \tag{3.30}$$

where in the vicinity of the source the pressure filed takes the form of the spherical Green's function. If $|p| = \frac{P_0}{4\pi}$ is required at $R = R_0$, then let $a = P_0 R_0$ and therefore

$$p = \frac{a}{4\pi R}e^{ik_0 R}, \tag{3.31}$$

where $R = \sqrt{r^2 + z^2}$. The source is represented as a point source at $(0, z_s)$ by

$$\Psi(r = 0, z) = \alpha\delta(z - z_s) . \tag{3.32}$$

Integrating Eq. (3.30) over all depths of the real ocean results in

$$\alpha = a \lim_{r \to 0} P_0 \sqrt{\frac{r}{R_0}} \int_0^\infty \frac{1}{4\pi R} e^{ik_0 r} dz . \tag{3.33}$$

In the far-field, $r \gg z$, R may be approximated such that

$$R = \sqrt{r^2 + \bar{z}^2} \approx r + \frac{\bar{z}^2}{2r}, \quad \bar{z} = z - z_s \tag{3.34}$$

thus reducing Eq. (3.33) to

$$\alpha \approx \sqrt{R_0} \lim_{r \to 0} \frac{e^{ik_0 r}}{4\pi\sqrt{r}} \int_0^\infty e^{ik_0 \frac{\bar{z}^2}{2r}} dz = \sqrt{R_0} \lim_{r \to 0} \frac{e^{ik_0 r}}{2\pi\sqrt{r}} \sqrt{\frac{-2\pi r}{ik_0}} , \tag{3.35}$$

and leaving

$$\alpha = \sqrt{\frac{iR_0}{2\pi k_0}} . \tag{3.36}$$

Performing a Fourier transform of Eq. (3.32) with the influence of the image source included, and specifying the source in the k_z-domain yields

$$\hat{\Psi}(r = 0, k) = \alpha \int_{-\infty}^{\infty} [\delta(z - z_s) - \delta(z + z_s)] e^{-ik_z z} dz = -2i\alpha \sin(k_z z_s) . \tag{3.37}$$

Equation (3.37) states that the starting field, in the wavenumber representation, has constant amplitude modulated by a phase due to the interaction of the source and its image. This representation is consistent with an omnidirectional source that supplies equal energy to all wavenumbers.

Rather than setting the amplitude of this function to unity to ensure equal population of all directions, a smooth taper is used at high absolute wavenumber values to limit the angular dimension of the source and to reduce sidelobe influences. This is necessary due to the wide-angle approximation being valid to only approximately 40°, and due to the restriction on how large the finite FFT will allow k_z/k_0. The wide-angle source is modified to produce an accurate solution in the far-field (Thomson and Bohun, 1988) by

$$F(k_z) = \left(1 - \frac{k_z^2}{k_0^2}\right)^{-1/4}, (|k_z| < k_0). \qquad (3.38)$$

The limits on k_z are chosen as such since for $|k_z| > k_0$ the angles of propagation are imaginary. Therefore, the source function is tapered within the limits $\left|\frac{k_z}{k_0}\right| < 1$.

Finally, to account for the half-mesh symmetry of the depth grid a phase term in the wavenumber domain of $e^{ik_z\frac{\Delta z}{2}}$ is added. The wavenumber domain starting field for the wide-angle point source can then be written as

$$\hat{\Psi}(r = 0,k_z) = -2i\sqrt{\frac{iR_0}{2\pi k_0}}\sin(k_z z_s)\left(1-\frac{k_z^2}{k_0^2}\right)^{-1/4} e^{ik_z\frac{\Delta z}{2}}. \tag{3.39}$$

Following Tappert's procedure, for the COIPE it is easiest to generate the starting field in the tilde domain. The starting depth, z_s, must then be transformed to tilde space. Defining

$$f = \frac{z_s - z_{j-1}}{z_j - z_{j-1}}, \tag{3.40}$$

the source depth in the tilde-domain is then

$$\tilde{z}_s = \tilde{z}_{j-1} + (\sqrt{c_j} + \sqrt{c_{j-1}})f\frac{z_j - z_{j-1}}{\sqrt{u_j} + \sqrt{c_{j-1}}} \tag{3.41}$$

where

$$u_j = fc_j + (1-f)c_{j-1}. \tag{3.42}$$

Note that Eq. (3.42) performs a linear interpolation of c at the source depth. Since, from Eq. (3.22)

$$\tilde{z}_j - \tilde{z}_{j-1} = 2\sqrt{c_0}\frac{z_j - z_{j-1}}{\sqrt{c_j} + \sqrt{c_{j-1}}}, \tag{3.43}$$

then Eq. (3.41) becomes

$$\tilde{z}_s = \tilde{z}_{j-1} + \frac{2\sqrt{c_o}(\tilde{z}_j - \tilde{z}_{j-1})f}{\sqrt{u_j} + \sqrt{c_{j-1}}} = \tilde{z}_{j-1} + \frac{2\sqrt{c_o}(z_s - \tilde{z}_{j-1})}{\sqrt{u_j} + \sqrt{c_{j-1}}} \tag{3.44}$$

or

$$\tilde{z}_s = \tilde{z}_{j-1} + \frac{2\sqrt{c_o}(z_s - \tilde{z}_{j-1})}{\sqrt{c_s} + \sqrt{c_{j-1}}}, \tag{3.45}$$

which is merely Eq. (3.19) rewritten using $c_s = c(z_s)$. Also from the expression for the tilde domain transformation,

$$\tilde{z} = \int_0^z \sqrt{n(z', r)}\,dz', \tag{3.46}$$

it follows that

$$\frac{d}{dz}\tilde{z} = \sqrt{n(z, r)} \quad . \tag{3.47}$$

Therefore,

$$\frac{dz}{d\tilde{z}} = (n(z, r))^{-1/2} \tag{3.48}$$

so

$$z = \int_0^{\tilde{z}} (n(z, r))^{-1/2} d\tilde{z}'. \tag{3.49}$$

Since $c(z) = c(z)$, then $n(z) = n(z)$, such that

$$z = \int_0^{\tilde{z}} (\tilde{n}(\tilde{z}', r))^{-1/2} d\tilde{z}' = \frac{1}{\sqrt{c_0(r)}} \int_0^{\tilde{z}} \sqrt{\tilde{c}(\tilde{z}')} d\tilde{z}' . \tag{3.50}$$

Equation (3.50) could be solved numerically, but it does not have the analytical expression the previous transformation did. Rather, the previous transformation for source depth can be applied to receiver depths at the original gridding of the environment. In other words, consider

$$z_k = \left(k - \frac{1}{2}\right)\Delta z \tag{3.51}$$

which is essentially what was obtained in Eq. (3.19), where now the tilde depths are those found in the original transformation vector, z_j for $j = 2 \ldots Ns-1$. Below z_{Ns-1}, $z_{k \geq Ns-1}$ is used.

To obtain the field, however, it must be noted that

$$\tilde{\Psi}(\tilde{z}, r) = [n(z, r)]^{-1/4} \Psi(z, r) \tag{3.52}$$

or, since $n(z) = n(z)$,

$$[\tilde{n}(\tilde{z}, r)]^4 \tilde{\Psi}(\tilde{z}, r) = \Psi(r) . \tag{3.53}$$

In either case, $\tilde{\Psi}(\tilde{z}_j)$ must first be interpolated from $\Psi(\tilde{z}_k)$. Since there is no simple gradient structure for $\Psi(\tilde{z})$, a

numerical scheme must be used. For this case, a typical 5-point interpolation scheme is used to obtain $\Psi(\tilde{z}_j)$. If Eq. (3.52) is used, then $n(z_k, r)$ is evaluated and the values of

$$\Psi(z_k, r) = [n(z_k, r)]^4 \Psi(\tilde{z}_j) \tag{3.54}$$

are computed where $k = j - 1$ and $c(z_k)$ is evaluated from the original profile. Note that $[\tilde{n}(\tilde{z}_k, r)]^4 \Psi(\tilde{z}_k)$ could have been computed and then interpolated to z_j. However, this would only be an approximate interpolation of n. Therefore, the former method is an exact interpolation of n and only approximate in Ψ, which is expected to be the more accurate method.

As was briefly discussed in the previous chapter, the COIPE approach is expected to remove the reference sound speed ambiguity present in the WAPE. Removing this sensitivity should provide more accurate results without the need to determine an appropriate reference sound speed for the specific problem. In the following chapter the COIPE is benchmarked against the SPE, WAPE, and normal mode theory.

IV. NUMERICAL RESULTS

The previous chapters present an outline of the historical and theoretical background of the parabolic equation approximation to the acoustic wave equation as well as the COIPE implementation. In this chapter, the focus shifts to the analysis of attempts to improve the accuracy and validity of the WAPE approximation. First, the effects of improving the numerical accuracy of the WAPE, as implemented by the MMPE model, is evaluated. Second, the COIPE implementation is evaluated under a number of test cases. Finally, the SPE, MMPE, and COIPE are subjected to the normal mode decomposition technique previously discussed.

A. DOUBLE-PRECISION IMPLEMENTATION OF THE MMPE

While the MMPE has been used successfully under a wide variety of test cases and environments for a number of years, it was recently tested extensively on a number of specific problems. These tests were conducted as part of the Shallow Water Acoustic Modeling (SWAM) Workshop held at the Naval Postgraduate School in 1999. The SWAM workshop provided a set of detailed environmental cases that served as the basis

for comparison between the numerous modeling efforts being undertaken in the United States and internationally. As part of this workshop, the convergence sensitivity of the MMPE to the choice of the range step, Δr, was analyzed (Smith, 2000). As a result of this analysis, which is discussed in more detail later in this section, an effort to develop a more numerically precise MMPE implementation was undertaken. Increasing the numerical precision of the model would also help answer whether truncation of the field, as postulated in the introduction, is a source of error in the model.

In an effort to avoid introducing new errors or anomalies into the MMPE, no algorithm changes were made to the program code itself. Rather, the variables and array declarations, as well as the corresponding post processing routines, were recast as double-precision. The original MMPE code was, with the exception of the FFT subroutine, predominantly single-precision. One of the concerns raised by this procedure was that computational times would increase dramatically. This, however, was not the case. Since the bulk of the computational work is done by the FFT subroutine, which was already in double-precision format, computational

times only increased by three to five percent. These increases are deemed relatively insignificant and do not in and of themselves hinder the use of the double-precision MMPE (DP-MMPE).

As a method of comparison with the SPE and existing MMPE, the DP-MMPE was tested using one of the SWAM test cases. The test case chosen was referred to as SWAM Flat-a. The environment has an isospeed water column, $c_0 = 1500$ m/s $\rho_0 = 1.00$ g/cm^3, overlying a flat bottom. The bottom properties are defined every 2 km and are linearly interpolated out to a range of 20 km. Compressional attenuation is fixed at 0.1 dB/λ and there is no shear in the bottom. The source is at a depth of 30 m and a frequency of 250 Hz CW. The environment is shown below in Fig. 4.1. Fig. 4.2 shows the full, CW field at 250 Hz for the source at 30 m as obtained from using the MMPE model solution.

During the theoretical development of the wide-angle PE approximation it was noted that the range step size Δr, as based on the centered-step scheme, is roughly third order accurate. The implications of this fact are that as the range step size is decreased, the solution accuracy should

improve until a stable solution converges. In fact, most PE models do follow this behavior. The PE/SSF does not.

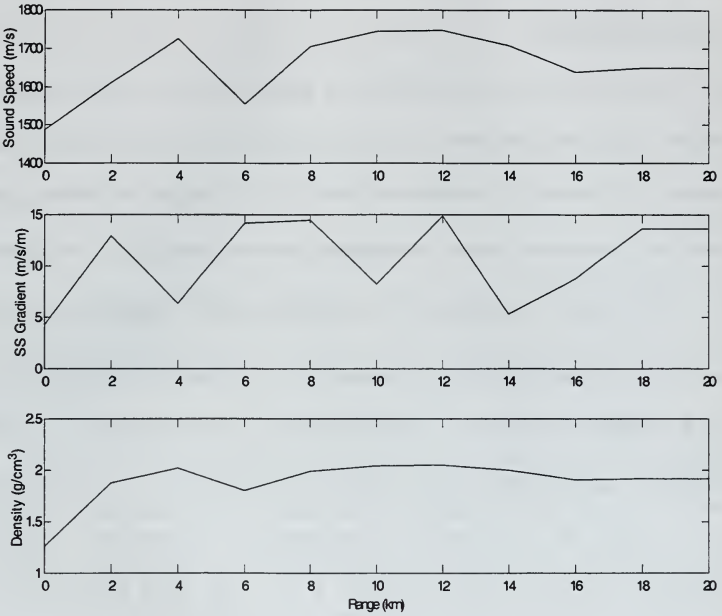

Figure 4.1. The Flat-a test case environment.

To illustrate the relation between the range-step size and the covergence of the solution, a number of solutions were generated for the Flat-a case discussed above. The only parameter varied in any of the cases was the size of the range-step. In each of the cases the transmission loss (TL)

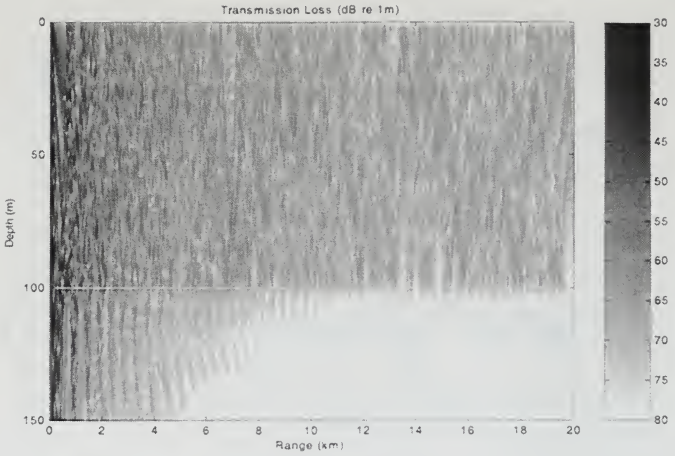

Figure 4.2. MMPE field solution for Flat-a case.

for a receiver at 35 m is shown in Fig. 4.3. The upper and lower panels of Figs. 4.3 and 4.4 show the first and last 5 km of the solution, respectively. Note that the solution appears to be converging as $\Delta r \sim 5$ m. As can be seen in Fig. 4.4, however, the solution diverges for further decrease of Δr; the solution degrades for values of Δr less than about 5 m. The solution appears to reach convergence at $\Delta r \sim \lambda$.

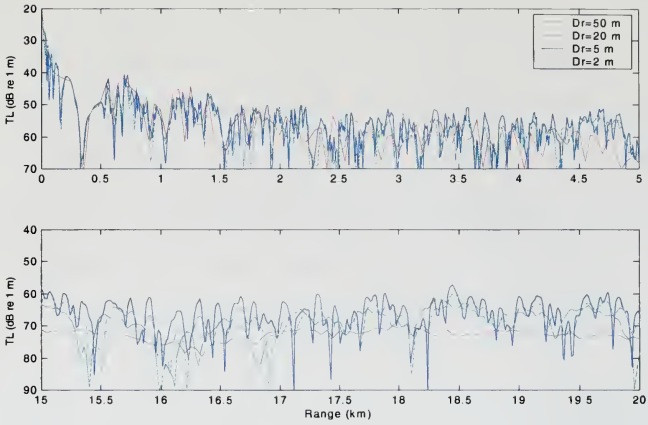

Figure 4.3. Convergence testing for various range-steps.

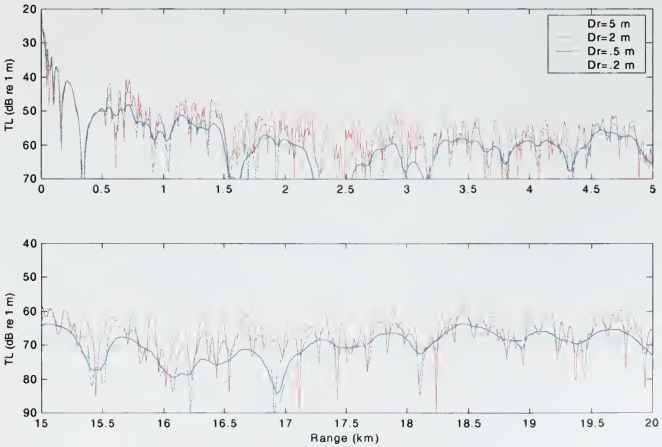

Figure 4.4. Stability testing for various range-steps.

A possible cause of this divergence was postulated to be truncation of the field and a lack of numerical precision in the declaration of variables in the MMPE computer code. In an effort to test this theory the DP-MMPE model was run with identical model inputs to those used in the convergence and stability testing shown above for the MMPE. The results of this testing are shown below in Figs. 4.5 and 4.6.

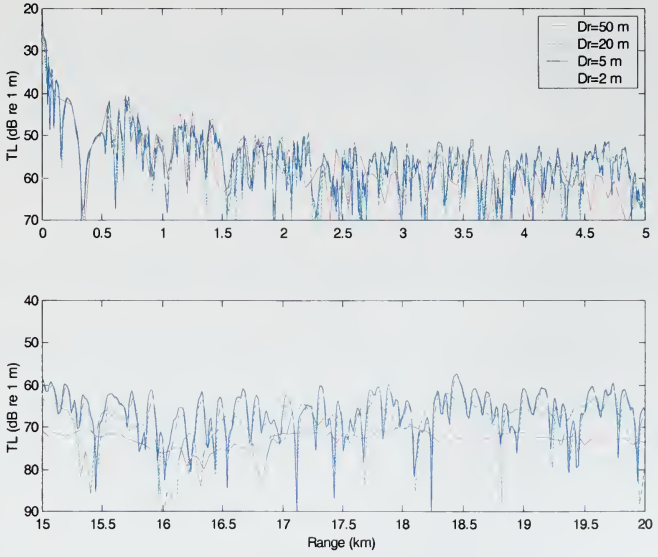

Figure 4.5. DP-MMPE convergence testing for various range-step sizes.

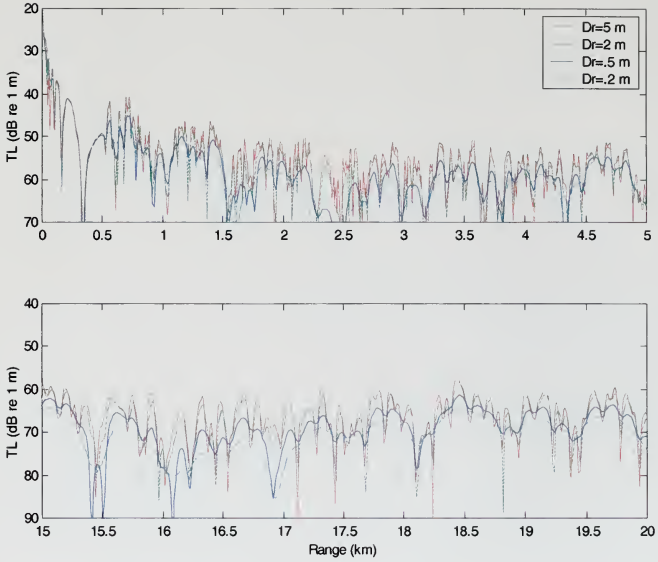

Figure 4.6. DP-MMPE stability testing for various range-step sizes.

Clearly, there does not appear to be any discernible improvement in the convergence of the solution through the use of the DP-MMPE. It exhibits the same general behavior as that of the original MMPE model. A comparison between the MMPE and DP-MMPE at the 5 m and 2 m range-step sizes is shown below in Fig. 4.7.

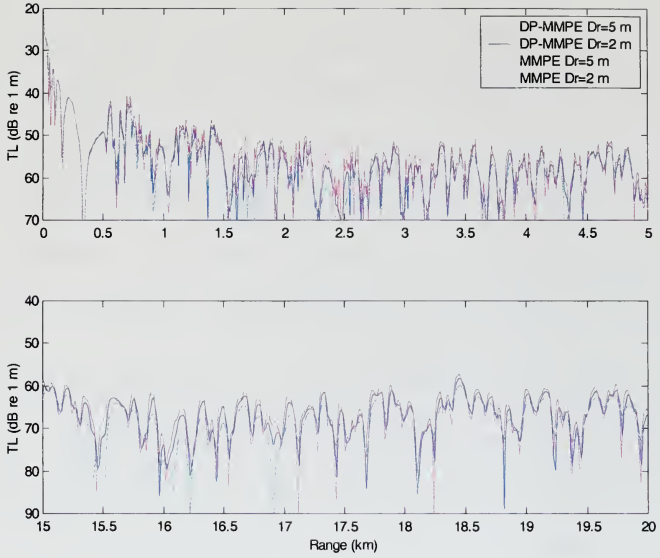

Figure 4.7. DP-MMPE and MMPE comparison for range-step sizes of 5 m and 2 m.

Referring to Fig. 4.7, it can be seen that for a range step size of 5 m the solution produced by the two models are indeed overlapping. For a range-step size of 2 m the two solutions differ slightly with range, with the DP-MMPE appearing to diverge less at some range points. One may conclude, however, that while the DP-MMPE does no worse, it does

not offer a solution as to why the PE/SSF algorithm seems to have a lower limit on the size of the range-step.

As a result of separate analysis (Smith, 2000), the primary cause of this non-convergence was found to be related to the structure of the propagator functions. Recall that the environmental propagator function is of the form $e^{-ik_0 \Delta r U_{op}(r,z)}$, and the wavenumber propagator function is of the form $e^{-ik_0 \Delta r T_{op}(k_z)}$. The wavenumber propagator decays exponentially beyond $k_z > k_0$. From this analysis it can be shown that the PE/SSF algorithm, for large range-step size, attempts to include a large amount of phase information into each range-step. If Δr is chosen to be too large, then errors are generated in the solution. Conversely, as Δr is reduced in size there is inadequate phase information contained in each range-step and the solution once again becomes inaccurate. The most accurate solutions may be expected for range-steps where a full cycle of phase information is contained in each propagator. The level at which Δr appears to provide the greatest degree of convergence is $\Delta r \sim \lambda$ (Smith 2000) for shallow water environments such as tested here.

Before leaving the area of solution convergence based on the range-step size, a final comparison between the MMPE and the COIPE is made. While the COIPE model was not implemented specifically to address this problem, it is of interest as to whether any of the changes made in the COIPE affect the convergence due to Δr. Below, in Fig. 4.8, the COIPE model is compared against the MMPE for the same test case used above. The MMPE results were chosen over the DP-MMPE since the DP-MMPE solutions did not offer any definitive advantages over the normal implementation. As Fig. 4.8 shows, the COIPE does not appear to offer any greater degree of convergence for the given Δr sizes in this environment. These results are inconclusive in regards to the COIPE model, but the implementation was not expected to affect the Δr sensitivity.

Finally, as a means of comparison against another modeling technique for this test case, the MMPE results for range-step size 5 m are compared to those developed by Mikhin (2000) for SWAM. These results were chosen as a benchmark due to the high degree of agreement with several test cases and several modeling techniques.

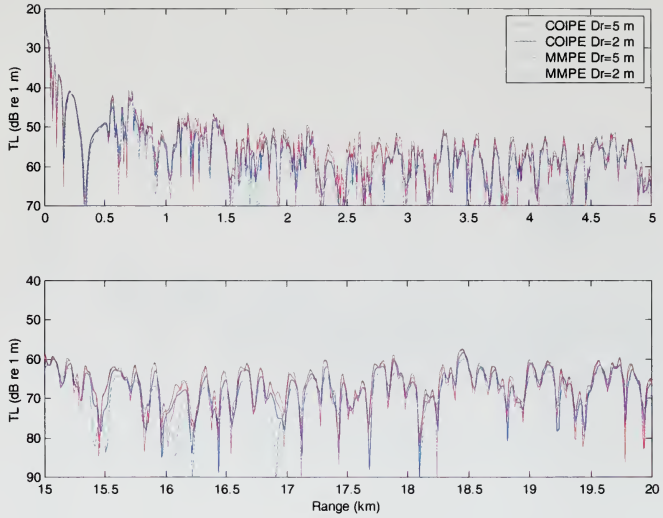

Figure 4.8. COIPE and MMPE convergence testing.

The comparison of the MMPE solution with the solution provided by Mikhin is shown below in Fig. 4.9. Solutions for rang-step sizes of 20, 5, and 2 m were chosen to demonstrate the degree of convergence with the reference solution for varying Δr. The figure shows very good agreement between the MMPE and Mikhin solutions at short ranges. The two tech-

niques show a greater degree of separation with increasing range. This is most likely the result of cumulative phase errors inherent to the wide-angle PE technique employed here. The figure also demonstrates, once again, that the

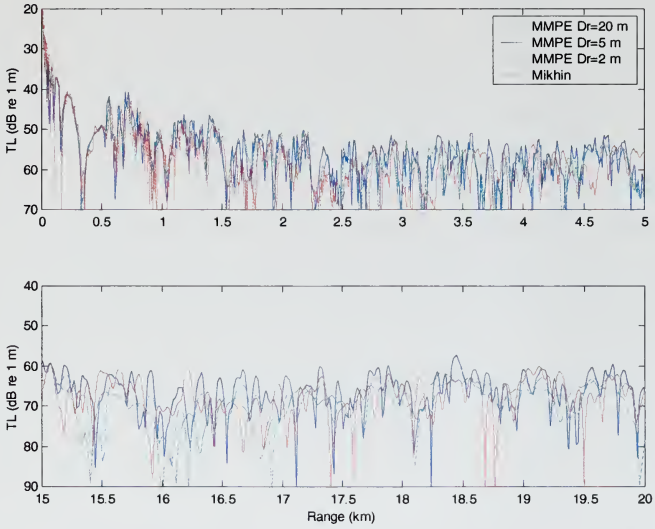

Figure 4.9. MMPE and Mikhin solution comparison for various range step-sizes.

choice of a 5 m range-step size provide the greatest degree of agreement with the reference solution.

B. THE COIPE IMPLEMENTATION OF THE MMPE

As was discussed in the last chapter, the COIPE model was developed by Tappert (1995) in an attempt to remove or reduce the dependence of the wide-angle PE approximation on the choice of the reference sound speed value while increasing the overall accuracy of the model. While this sensitivity has been observed in a number of test cases, it was extensively studied during one of the PE Workshop II (PE-II) test cases (Porter and Jensen, 1993). This case, referred to as the Porter duct problem, was based on the observation that many of the wide-angle split-step PE approximations overestimated the value of the TL when applied to long-range propagation in a leaky surface duct environment. The SPE implementation of the PE/SSF algorithm does not generate this anomaly. Additionally, other PE implementations based on Pade' series expansions of the square root operator (which maintain the proper normal mode basis set) do not result in this overestimation of the downrange TL. The results of PE-II showed that many wide-angle models that do not use the Thomson-Chapman (TC) wide-angle approximation avoid this problem.

The Porter duct environment is one of a source and receiver located in a 250 m deep surface duct. The source is at a depth of 25 m and frequency of 80 Hz. The receiver is at a depth of 100 m. The ocean bottom is range-independent with a lossy fluid half-space beginning at a depth of 4 km. Of the 78 propagating modes in the water column, one is trapped in the surface duct. Figures 4.10 and 4.11 illustrate the sound speed profile and TL field for this environment respectively.

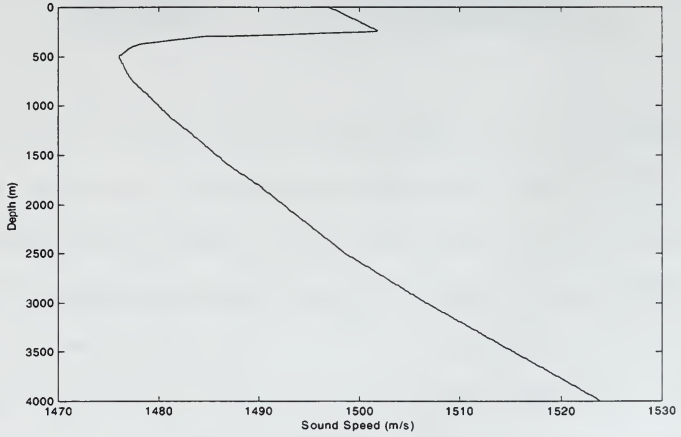

Figure 4.10. Porter duct sound speed profile plot.

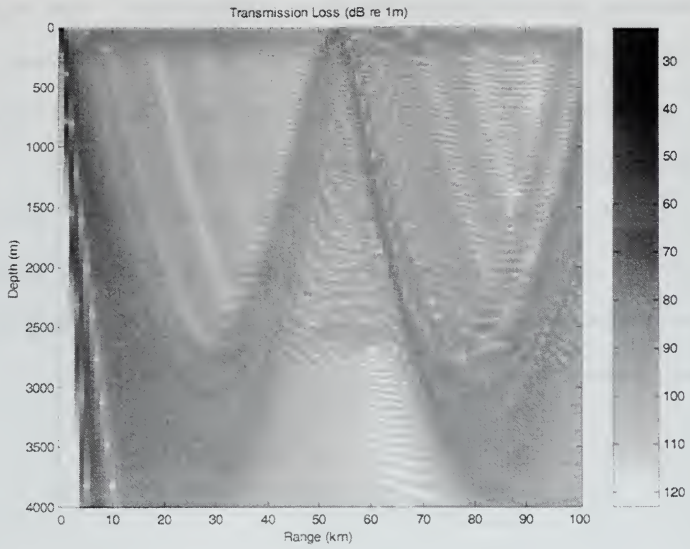

Figure 4.11. TL field plot for the Porter duct problem.

Finn Jensen, during PE Workshop II, showed that the SPE was in excellent agreement with the normal mode reference solution used in the test case (Porter and Jensen, 1993). Because this reference solution is no longer available, the SPE results were used as the reference for this analysis. The only alterations to the various model input parameters changed in the following analysis is that of the reference sound speed, c_0. Prior to looking at the COIPE model or the

effects of varying c_0, the TL plot for the receiver depth of 100 m is shown in Fig. 4.12 for the SPE and WAPE implementations when a reference sound speed of c_0 = 1500 m/s is used. It can be clearly seen that the WAPE solution shows a distinct drop off at ranges beyond about 60 km. It is this anomaly that the COIPE model is meant to eliminate.

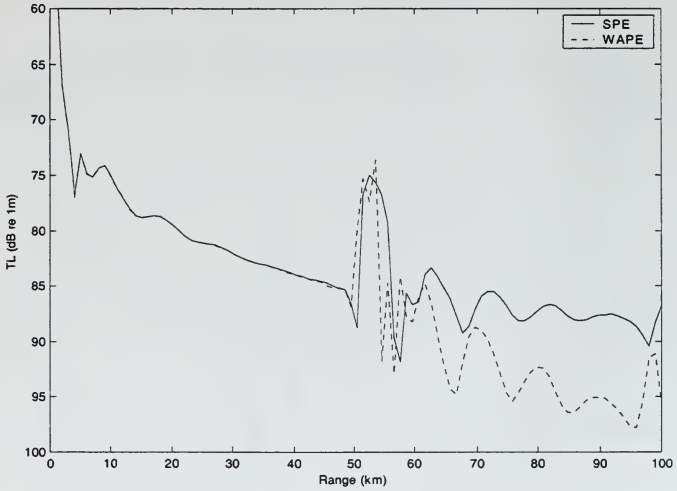

Figure 4.12. TL Plots for SPE and WAPE at the receiver depth of 100 m and c_0 = 1500 m/s.

The reference sound speed was then set at 1485 m/s and the two models were run again. These results are shown in

Fig. 4.13. This plot illustrates the effect the value of c_0 has on the WAPE solution. By "correctly" choosing the value of c_0, the WAPE correctly determines the long range TL. The difficulty, however, is in correctly determining this value. A change in c_0 by as little as 5 m/s to either side of this "correct" value results in the long range drop off shown in Fig. 4.12.

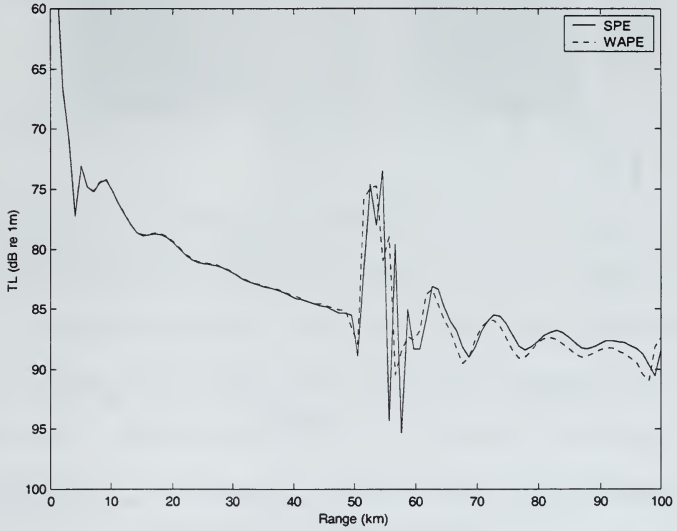

Figure 4.13. TL Plots for SPE and WAPE at the receiver depth of 100 m and c_0 = 1485 m/s.

The COIPE was then tested using identical environmental inputs to those used in the analysis above. COIPE model runs were made at c_0 values of 1500 and 1485 to provide comparison with the SPE results. These are shown in Figs. 4.14 and 4.15 respectively. The COIPE model compares well with the SPE solution at all ranges and there is no drop off at extended range as was observed with the WAPE. The COIPE solution is indeed insensitive to changes in the reference sound

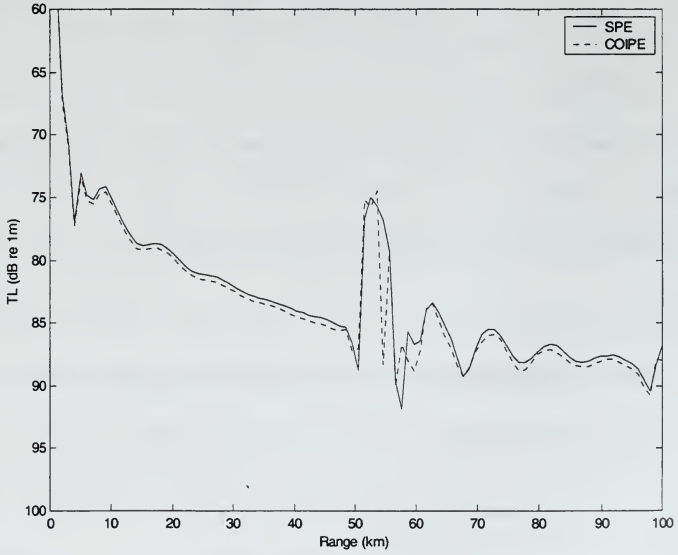

Figure 4.14. TL Plots for SPE and COIPE at the receiver depth of 100 m and c_0 = 1500 m/s.

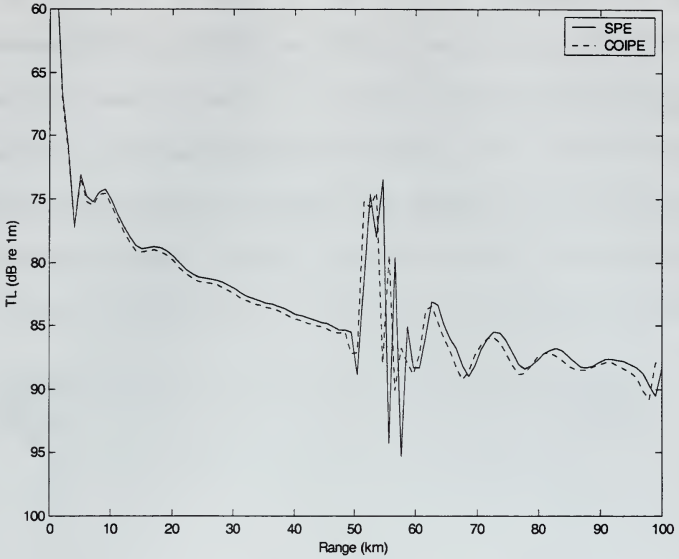

Figure 4.15. TL Plots for SPE and COIPE at the receiver depth of 100 m and c_0 = 1485 m/s.

speed, as shown in Fig. 4.15. While both plots in Fig. 4.15 do show phase differences from those of Fig. 4.14, the COIPE follows the reference solution equally well in both cases. The COIPE was tested at a wide variety of c_0 values with similarly successful results.

Clearly the COIPE corrects the TL drop-off encountered in the MMPE and similar wide-angle implementations. The

COIPE corrects the small error in the phase calculation caused by the incorrect choice of the reference sound speed. A small error in this phase calculation can cause a large, on the order of 20 dB, downrange TL error (Porter and Jensen, 1993). The test case highlights this problem because it supports a single trapped mode in the surface duct that is a leaky mode. The trapped mode continually loses energy into the lower region where, due to the strong upward refracting profile, it is directed back up toward the surface duct causing interferences. Small phase errors result in incorrectly applying these interferences to the surface duct mode. The transformation and subsequent calculation of the reference sound speed at each range step removes the source of these phase errors and thus correctly applies the interferences described above.

C. NORMAL MODE DECOMPOSITION OF THE PE FIELD

The mode functions of the wide-angle PE approximation form a different basis set for modal expansion than those obtained using standard normal mode theory. As discussed in the theoretical development presented earlier, the SPE does reproduce the standard basis set. This section presents an

analysis and comparison of the modal decomposition of the SPE, WAPE, and COIPE models.

The ocean environment chosen for this analysis is the Munk canonical profile (Munk, 1974). This is a deep ocean, range-independent environment with sound speed profile characterized by

$$[c(z)-c_0]/c_0 = \varepsilon(e^{\eta}-\eta-1), \qquad (4.1)$$

where $\varepsilon = 0.0057$, the scaled depth variable $\eta = 2(z-z_{axis})/B$, and the reference sound speed is 1490 m/s. The axis depth was set at $z_{axis} = 1000\,m$, and the bottom depth at 4500 m. The sound speed profile is shown below in Fig. 4.16. The source was placed at a depth of 1000 m with a frequency of 100 Hz. A computational range of 100 km was used for PE field calculations. A bottom depth of 4500 m and a computational depth of 8000 m were used.

The acoustic pressure field was calculated using each of the three models. The field is shown in Fig. 4.17. The resulting fields were then decomposed into normal modes and the mode amplitudes determined using the techniques outlined in Chapter II for each of the models. Since the

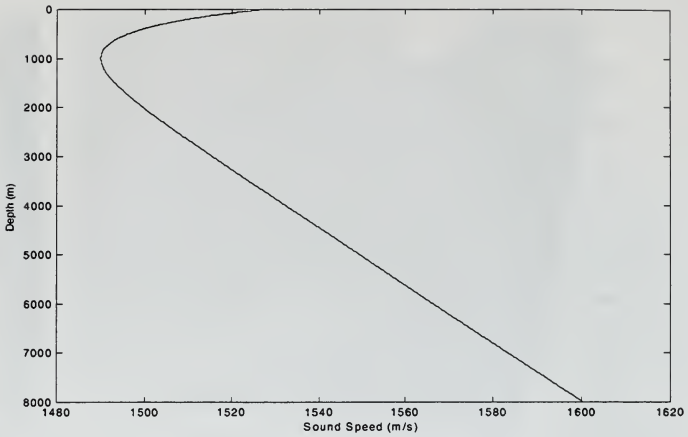

Figure 4.16. Munk canonical sound speed profile.

environment chosen is range-independent, the mode amplitudes should remain constant with range. The amplitudes for selected modes are shown in Figs. 4.18 thru 4.20 for the SPE, WAPE, and COIPE respectively. Modes were chosen to avoid overlapping plots to improve readability and to avoid bottom interactions. The reference sound speed is 1500 m/s for this series of plots. Each of the three models produce satisfactory results for the lower modes. Note the nearly constant

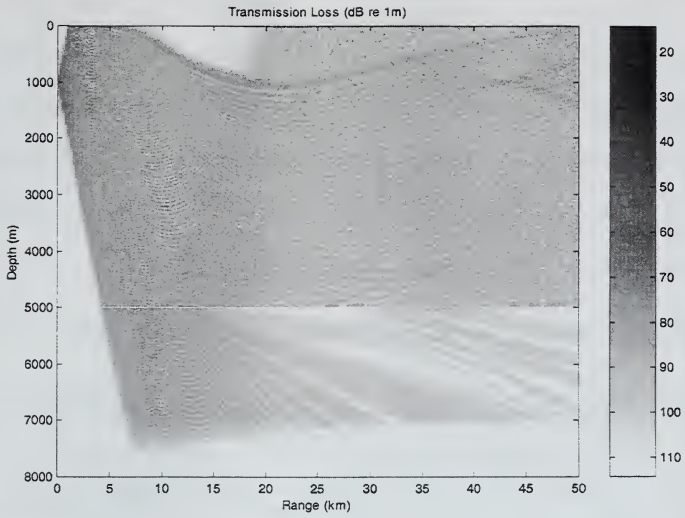

Figure 4.17. TL Field plot for Munk canonical profile.

amplitude with range for all three models. The higher order modes of the WAPE plot, however, show increasing levels of fluctuations. Conversely, the COIPE modal amplitudes compare well with the SPE results and do not show the high degree of fluctuation seen in the WAPE plots.

The three models were then tested for this environment using a reference sound speed of 1490 m/s. The results are shown in Figs. 4.21 through 4.23. The results for the COIPE, Fig. 4.23, are visibly unchanged, as expected. The WAPE

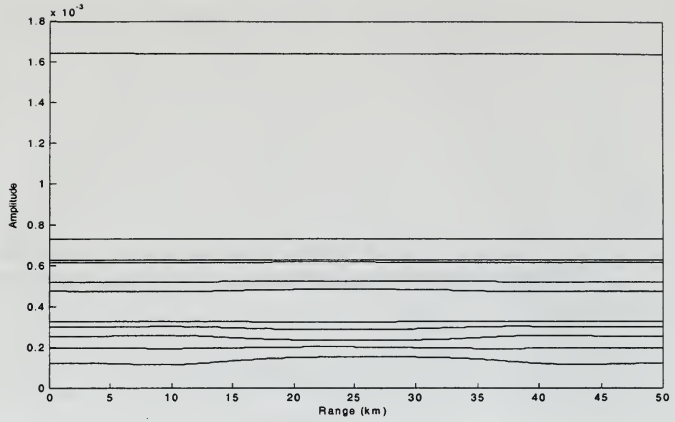

Figure 4.18. SPE mode amplitudes with range for modes 1, 5, 10, 15, 20, 25, 30, 35, 40, 45, and 50. (c_0 = 1500 m/s)

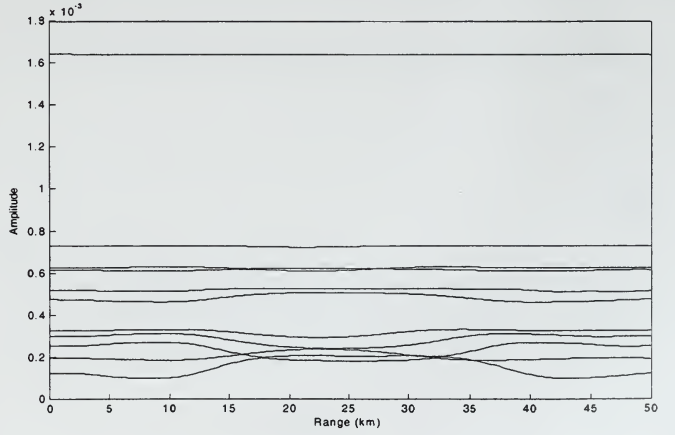

Figure 4.19. WAPE mode amplitudes with range for modes 1, 5, 10, 15, 20, 25, 30, 35, 40, 45, and 50. (c_0 = 1500 m/s)

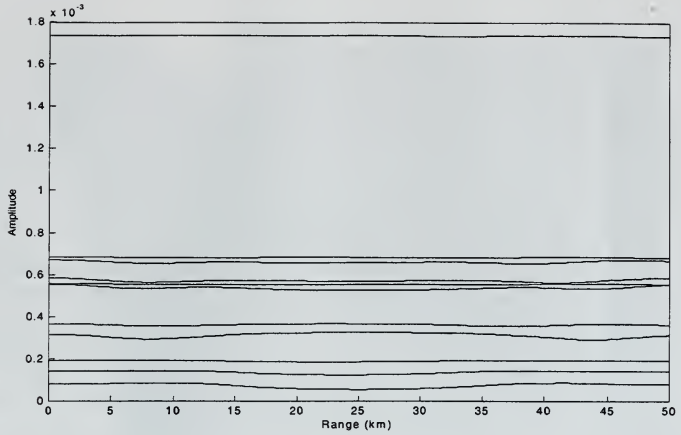

Figure 4.20. COIPE mode amplitudes with range for modes 1, 5, 10, 15, 20, 25, 30, 35, 40, 45, and 50. (c_0 = 1500 m/s)

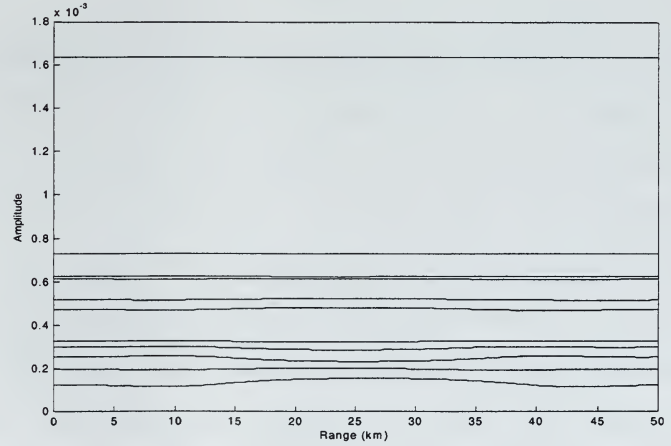

Figure 4.21. SPE mode amplitudes with range for modes 1, 5, 10, 15, 20, 25, 30, 35, 40, 45, and 50. (c_0 = 1490 m/s)

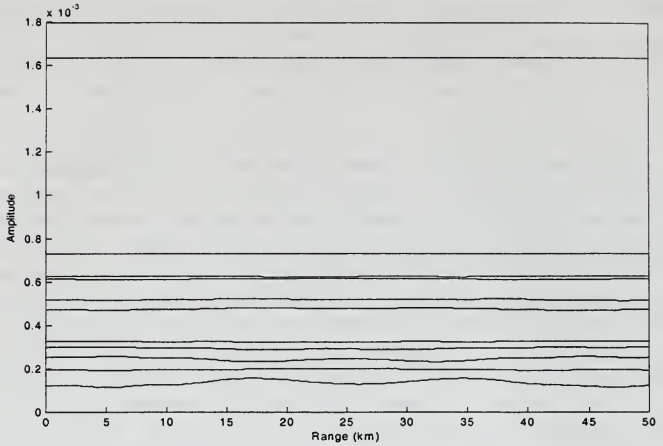

Figure 4.22. WAPE mode amplitudes with range for modes 1, 5, 10, 15, 20, 25, 30, 35, 40, 45, and 50. (c_0 = 1490 m/s)

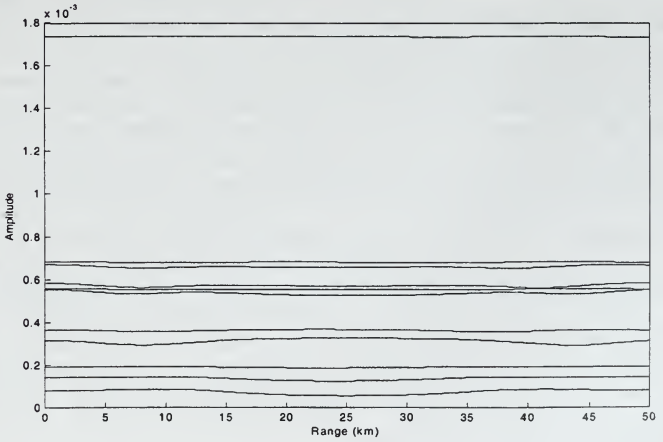

Figure 4.23. COIPE mode amplitudes with range for modes 1, 5, 10, 15, 20, 25, 30, 35, 40, 45, and 50. (c_0 = 1490 m/s)

amplitudes show somewhat less fluctuation for the higher modes. This can most likely be attributed to the sensitivity to the reference sound speed discussed in the previous section.

This analysis has demonstrated the wide-angle PE's lack of the ability to reproduce the standard normal mode basis set as defined by normal mode theory and as duplicated by the SPE. The WAPE shows increasing levels of fluctuation in the modal amplitudes with increasing mode numbers. This fluctuation results in the produced PE field not exactly representing the environment under study. The COIPE, however, does not show the same degree of fluctuation in modal amplitudes, and therefore should better represent the acoustic field. It should be noted that the modal amplitudes of the COIPE do not exactly match those of the SPE. This is due to the generation of the source function in the tilde-domain. A more proper treatment might generate the starting field in real space and then transform to tilde space. However, this would introduce some numerical errors to the transformation of the filed form tilde to real space. This is an area for further analysis and study.

V. CONCLUSIONS AND SUMMARY

This thesis has examined the parabolic equation approximation to the acoustic wave equation and, in particular, two possible implementations aimed at removing inherent WAPE errors were analyzed. The theoretical background underlying each of these models was presented along with the specific numerical implementation used for testing and comparison with existing PE approximations. Finally, numerical results were provided comparing the SPE, WAPE, DP-WAPE, and COIPE models against a number of test cases. These included results from the SWAM workshop, the Porter duct problem, and the Munk canonical profile.

The parabolic equation and many of its derivatives suffer from a number of anomalies or errors depending on the particular implementation being used. Of these, three were examined in this analysis. First, the selection of the range-step size used by the PE/SSF algorithm affects both the convergence and the stability (Smith, 2000) of the solution with an error to second or third order in the range-step increment (Jensen, et. al., 1994). Second, the WAPE suffers an anomaly that under certain environmental conditions it

incorrectly computes the down-range TL (Porter and Jensen, 1993). This anomaly is manifest in a distinct drop in TL. Results of the Parabolic Equation Workshop II (PE-II) attribute this error to incorrectly handling the loss of energy from a leaky surface duct mode and its subsequent interaction with the remaining sound field. It was shown here, and in PE-II, that the manifestation of this anomaly is highly dependent on the choice of the reference sound speed. A small change in the value of c_0 results in a significant change in the computed down-range TL. Third, the WAPE does not reproduce the standard normal mode basis set as defined by normal mode theory and as reproduced by the SPE. In addition to the phase errors experienced to some degree by all PE approximations, the WAPE mode amplitudes exhibit a range dependence in a range-independent environment (Smith and Smith, 1997). This effect was found to contribute to the anomalous TL findings just described.

A double-precision version of the WAPE model was implemented in an attempt to remove or improve the convergence sensitivity to the selection of the range-step size used by the PE/SSF algorithm. The double-precision model was tested against the existing SPE, WAPE, and COIPE models in a simple

range-dependent environment originally defined for SWAM. The double-precision model was found to do as well as, but no better than, the existing approximations under the tested conditions. From this analysis it was concluded that the range-step convergence sensitivity is inherent to the PE/SSF algorithm used by the models. This is supported by separate analysis done by Smith (2000). The most accurate solutions may be expected for range-steps where a full cycle of phase information is contained in each of the propagators used by the algorithm. The level at which Δr appears to provide the greatest degree of convergence is $\Delta r \sim \lambda$ (Smith 2000) for shallow water environments such as those tested. The COIPE model was also tested for sensitivity to the choice of the range-step on solution convergence. It was found to be similarly affected, as was expected.

The COIPE model, a WAPE implementation, was developed to remove or reduce the solution sensitivity to the choice of the reference sound speed value (Tappert, 1991). The COIPE model uses an operator transformation which results in a range-dependent series of values for the reference sound speed. The COIPE model was compared with the SPE and WAPE models using the Porter duct problem developed for PE-II

(Porter and Jensen, 1993). These tests were conducted using a variety of reference sound speed values, with successful results in all cases. The COIPE model does not exhibit the TL drop with range seen with the WAPE.

Finally, the COIPE was tested against the SPE and WAPE models for its ability to decompose properly into the standard mode basis set. The models were tested in a deep-ocean Munk canonical profile environment. As discussed, the WAPE does not correctly decompose with this basis set, and shows a range dependence in its modal amplitudes in a range-independent environment. This range dependence can be seen as fluctuations in the modal amplitudes with range. The COIPE modal amplitudes show much less fluctuation with range than those of the WAPE, and more closely reproduce those obtained by the SPE. This is a result of the improved handling of the phase by the COIPE as outlined above and demonstrated through the modal decomposition.

The double-precision model testing provides further evidence, in addition to that shown by Smith (2000), that the small range-step sensitivity is a fundamental property of the PE/SSF algorithm, and no further investigation of this property is necessary. The results of the COIPE model test-

ing, while promising, are not conclusive. The COIPE corrects the error seen in the Porter duct problem, and improves the reproduction of the standard normal mode basis set, but requires further investigation. Preliminary testing in shallow water environments indicate the COIPE may not produce results significantly different from those of the WAPE model. Additionally, the mode amplitudes themselves, while showing less fluctuations, are of different relative magnitudes from those produced by the SPE. This remains as an area for further investigation.

THIS PAGE INTENTIONALLY LEFT BLANK

LIST OF REFERENCES

Bellman, R., (**1964**). *Perturbation Techniques in Mathematics, Physics, and Engineering* (Holt, Rinehart, and Winston, Inc., New York), pp. 38-39.

Collins, M. D., (**1994**). "Generalization of the Split-Step Pade Solution," J. Acoust. Soc. Am. **96**, pp. 382-385.

Fock, V. A., (**1965**). *Electromagnetic Diffraction and Propagation Problems* (Pergamon, New York).

Hardin, R. H. and Tappert, F. D., (**1973**). "Applications of the Split-Step Fourier Method to the Numerical Solution of Nonlinear and Variable Coefficient Wave Equations," SIAM Rev. **15**.

Jensen, F. B., Kuperman, W. A., Porter, M. B., and Schmidt, H., (**1994**). *Computational Ocean Acoustics* (AIP, New York).

Lee, D., Botseas, G. and Papadakis, J. S., (**1981**). "Finite-Difference Solution to the Parabolic Wave Equation," J. Acoust. Soc. Am. **70**, pp. 795-800.

Leontovich and Fock, V. A., (**1946**). *Zh. Eksp. Teor. Fiz.* (Sov. Phys. JETP, Moscow), pp. 13-24.

McDaniel, S. T., (**1975**). "Propagation of Normal Modes in the Parabolic Approximation," J. Acoust. Soc. Am. **57**, pp. 307-311.

McDaniel, S. T., (**1975**). "Parabolic Approximations for Underwater Sound Propagation," J. Acoust. Soc. Am. **58**, pp. 1178-1185.

Mikhin, D., (**1999**). "Energy-Conserving and Reciprocal Solutions for Higher-Order Parabolic Equations," unpublished report from Shallow Water Acoustic Workshop.

Munk, W. H., (**1974**). "Sound Channel in an Exponentially Stratified Ocean, with Application to SOFAR," J. Acoust. Soc. Am. **55**, pp. 220-226.

Porter, M. B., and Jensen, F. B., (**1993**). "Anomalous Parabolic Equation Results for Propagation in Leaky Surface Ducts," J. Acoust. Soc. Am. **94**, pp. 1510-1516.

Smith, A. R., and Smith, K. B., (**1997**). "Mode Functions for the Wide-Angle Approximation to the Parabolic Equation," J. Acoust. Soc. Am. **103**, pp. 814-821.

Smith, K. B., (**2000**). "Convergence, Stability, and Variability of Shallow Water Acoustic Predictions Using a Split-Step Fourier Parabolic Equation Model," unpublished report from Shallow Water Acoustic Workshop.

Smith, K. B., Brown, M. G., and Tappert, F. D., (**1992**). "Ray Chaos in Underwater Acoustics," J. Acoust. Soc. Am. **91**, pp. 1939-1949.

Tappert, F. D., (**1977**). "The Parabolic Approximation Method," in *Wave Propagation and Underwater Acoustics, Lecture Notes in Physics*, edited by J. B. Keller and J. S. Papadakis (Springer-Verlag, Berlin), Vol. **70**, pp. 224-287.

Tappert, F. D., (**1991**). "Density in PE/SSF," unpublished lecture notes.

Tappert, F. D., and Brown, M. G., (**1996**). "Asymptotic Phase Errors in Parabolic Approximations to the One-Way Helmholtz Equation," J. Acoust. Soc. Am. **99**, pp. 1405-1414.

Tappert, F. D., Spiesberger, J. L., and Boden, L., (**1995**). "New Full-Wave Approximation for Ocean Acoustic Travel Time Predictions," J. Acoust. Soc. Am. **97**, pp. 2771-2782.

Thomson, D. J., (**1993**). "PE-Based Spectral Decomposition," in *PE Workshop II: Proceedings of the Second Parabolic Equation Workshop*, edited by S. A. Cin-Bing, D. B. King, J. A. Davis, and R. B. Evans, Naval Research Laboratory NRL/BE/7181-93-001 (US Government Printing Office), pp. 296-320.

Thomson, D. J., and Bohun, C. S., (**1988**). "A Wide-Angle Initial Field for the Parabolic Equation Models," J. Acoust. Soc. Am. **83**, pg. S118.

Thomson, D. J., and Chapman, N. R., (**1983**). "A Wide-Angle Split-Step Algorithm for the Parabolic Equation," J. Acoust. Soc. Am. **74**, pp. 1849-1854.

THIS PAGE INTENTIONALLY LEFT BLANK

INITIAL DISTRIBUTION LIST

1. Defense Technical Information Center 2
   8725 John J. Kingman Rd., STE 0944
   Ft. Belvoir, Virginia 22060-6218

2. Dudley Knox Library 2
   Naval Postgraduate School
   411 Dyer Rd.
   Monterey, California 93943-5101

3. Prof. Kevin B. Smith 3
   Department of Physics, CODE PH/SK
   Naval Postgraduate School
   Monterey, California 93943-5117

4. Prof. James V. Sanders 1
   Department of Physics, CODE PH/SJ
   Naval Postgraduate School
   Monterey, California 93943-5117

5. Undersea Warfare Programs Office, Code 35 1
   833 Dyer Rd., Room 304
   Naval Postgraduate School
   Monterey, California 93943-5124

6. Kirk A. Weatherly, LT USN 2
   607 South Main Street
   Farmland, Indiana 47340

7. Joseph D. Weatherly 2
   St. Rd. 32 W, PO Box 202
   Farmland, IN 47340